Tilt Angle Optimization in Two-Tier Cellular Networks—A Stochastic Geometry Approach

Raul Hernandez-Aquino, Syed Ali Raza Zaidi, *Student Member, IEEE*, Des McLernon, *Member, IEEE*, Mounir Ghogho, *Senior Member, IEEE*, and Ali Imran, *Member, IEEE*

***Abstract*—In this work, we address the antenna tilt optimization problem for a two-tier cellular network consisting of macrocells and femtocells, where both tiers share the same spectrum and their positions are modeled via two independent Poisson point processes (PPPs). First, we derive the coverage probability for a traditional cellular network consisting only of macrocells and obtain the optimum tilt angle that maximizes the overall energy efficiency (EE). Gains of up to 400% in EE were found for a scenario (approximately) equivalent to a hexagonal cell deployment with cell radius of 200 m when the optimum tilt was selected. We then proceed to model the heterogeneous network (HetNet) scenario where femtocells are also deployed in the network's area. We observe that the macrousers performance is highly sensitive to the interference emanating from the femtocell tier. In order to circumvent this issue, interference coordination employing a guard zone for the macrocell user is proposed. Subsequently, we formulate a joint optimization problem where we derive both, the radius of a guard zone protecting the macrouser and the tilt angle that maximize the EE of the network.**

***Index Terms*—Energy efficiency, Rayleigh fading, antenna tilt, Poisson point process (PPP).**

I. Introduction

THE energy efficiency (EE) of telecommunication systems is a major aspect that needs to be considered for future network deployments, as it has both economical and ecological repercussions. Therefore, new techniques and algorithms are being deployed in order to address these aspects. In this regard, the deployment of heterogeneous networks (HetNets) has the potential benefit of increasing the overall system coverage and throughput by placing tiers of several smaller cells. These smaller cells can provide service to specific areas with the advantage of having a smaller path loss given that the transmitting base stations are placed closer to the users [1]. However, a large scale and unplanned deployment of these smaller cells can incur a significant power penalty if the EE is not considered in the design of the HetNet.

On the other hand, in order to cope to the ever changing demands and configurations of a network, Self Optimizing Networks (SONs) are being studied for future network deployments [2]. In principle, a SON pursues the goal of adapting to the changes in the conditions of the network to provide good performance in a fast and flexible manner. The response to the environmental changes in a SON should be made in an acute manner (agility), in an acceptable period of time (stability), and regardless of the increase in the size or scale of the system (scalability). Among the solutions considered in the context of SONs, the antenna tilt angle has been proposed as a way of self optimizing a network. The antenna tilt, defined as the angle of the main beam of the antenna below the horizontal plane [3], has the potential to achieve gains in the performance of the network by focusing most of the power radiated into a desired location. Additionally, with the use of a remote electrical tilt (RET), a network can reconfigure itself. That way, the performance of the network can be greatly enhanced without the need to physically change the position of the antennas in the base stations (BSs). Moreover, the antenna tilting design has been recognized by industry as a powerful technique for future SONs due to its impact on both the interference, and the coverage as it is pointed out by JDS Uniphase Corporation in its white paper [4]. Furthermore, there have been extensive simulations in the past that have examined which antenna tilt angle provides the best gains for the network in terms of coverage and/or data rates. However, while considering a SON scenario, an open issue still remains as fast convergent algorithms are needed in order to cope with the rapid changes in network parameters. Moreover, it still remains unclear how the tilt angle should be adjusted in a HetNet to cope with the existence of other tiers of interferers in the network, while still achieving an acceptable performance.

Now, the use of stochastic geometry to model the behaviour of infrastructure-less networks such as ad-hoc and femtocell networks has been increasing over the past years and it has recently expanded to the case of HetNets, [5]–[9]. This is due to the fact that it provides a mean by which the behaviour of a network (where the nodes are randomly positioned) can be evaluated analytically and in a tractable manner. Hence, with the use of stochastic geometry, a network-wide characterization of the performance can be achieved. Therefore, in this work we

Manuscript received March 6, 2015; revised July 8, 2015 and September 20, 2015; accepted September 22, 2015. Date of publication October 2, 2015; date of current version December 15, 2015. This work was supported in part by CONACYT, Mexico, in part by the Secretaria de Educacion Publica, in part by the Mexican government, and in part by the U.S. Army Research Lab under Grant W911NF-13-1-0216. The associate editor coordinating the review of this paper and approving it for publication was M. Di Renzo.

R. Hernandez-Aquino, S. A. R. Zaidi, and D. McLernon are with the School of Electronic and Electrical Engineering, University of Leeds, Leeds LS2 9JT, U.K. (e-mail: elrha@leeds.ac.uk; s.a.zaidi@leeds.ac.uk; d.c.mclernon@leeds.ac.uk).

M. Ghogho is with the School of Electronic and Electrical Engineering, University of Leeds, Leeds LS2 9JT, U.K., and also with the Department of Electronics, Logistics, Informatics, and Telecommunications, International University of Rabat, Technopolis, Morocco (e-mail: m.ghogho@leeds.ac.uk).

A. Imran is with the Telecommunications Engineering Program, University of Oklahoma, Norman, OK 73019 USA (e-mail: ali.imran@ou.edu).

Color versions of one or more of the figures in this paper are available online at http://ieeexplore.ieee.org.

Digital Object Identifier 10.1109/TCOMM.2015.2485981

address the issue of determining the tilt angle that maximizes the EE of a two-tier network consisting of macrocells and femtocells when constraints on minimum Quality of Service (QoS) in each tier are considered. Employing well established tools from stochastic geometry, we model the positions of both, the macro base stations (MBSs) and the femtocell access points (FAPs) as independent Poisson Point Processes (PPPs). The use of PPPs to characterize the macrocell tier provides a lower bound on the actual performance of this tier with a tractable analytical framework [10]–[12]. This is in contrast with the typical hexagonal grid model, which provides an upper bound at the cost of tedious and time consuming simulations and/or numerical integrations. The proposed methodology takes into account the vertical pattern, while making use of the thinning property of a PPP to characterize the behaviour on the horizontal plane. Thus, the developed model provides a realistic, yet accurate 3-D representation of a system, considering the antenna pattern. With the proposed PPPs we can provide an analytical framework from which the overall performance of the network can be evaluated without the need to run time and resource consuming simulations. We first address the issue of tilt optimization for a traditional cellular network (only macrocells deployed). We show the existence of an optimum tilt angle that maximizes both the coverage probability and the EE. Then, we analyse the case of a two-tier HetNet where both macro- and femtocell tiers share the same spectrum. It turns out that the interference created by the femtocells has a great effect on the macrocell users' performance. In order to cope with this issue, we propose an interference coordination scheme in which a guard zone protecting the macrocell user is utilized. Accordingly, we formulate an optimization problem over a guard zone radius (protecting the macrocell users from femto interference) and the tilt angle that would maximize the EE of the network with constraints on the minimum coverage probability of each tier.

A. Related Work

There have been a number of papers considering the issue of the antenna tilt optimization for cellular networks. However, in order to characterize the performance of the network, most of them make use of time consuming simulations and have only studied the case of a traditional cellular network consisting of macrocells only. In [3], a comparison in terms of coverage is carried out between a system with mechanical tilt, electrical tilt and a combination of both. The network is modelled with a hexagonal grid and through simulations, the optimum tilt angle is found for scenarios with different inter-site distance. In [13], an optimization problem is proposed for a network with the presence of hotspots where a high number of users is identified. A hexagonal grid with cells having 3 sectors is assumed. The complexity of the original problem consisting of obtaining the tilt angle that maximizes the throughput of all users is first reduced by considering an optimization of the tilt over a center of gravity where a hot spot is located. Then, the system wide problem is decomposed into a local sub-problem which considers the triplet of adjacent (most interfering) sectors in order to find a decentralized solution. The same approach is followed in [14] but in the context of a network with macrocells and relays which are placed at random positions. At most one relay is placed in each base station sector to provide service where there is a coverage hole or where the concentration of users around that location forms a hotspot.

Now, in the case of HetNets, there are only a few works which consider the effect of the antenna tilt in the presence of other tiers of interferers. In [15] the issue of antenna tilt is addressed for both, a traditional network consisting of macro base stations and a HetNet considering the inclusion of femtocells to provide service to hotspots. The parameters used follow LTE specifications and the results are found via simulations. The emphasis of the work was to obtain a better performance in EE and throughput fairness (ratio of the cell edge users throughput to the cell mean user throughput). A reinforced machine learning algorithm is proposed, in which each base station individually can change its antenna tilt angle and the learning comes from observing the effects of the actions taken. In [16], direct and indirect (learning theory and game theory) biomimetrics approaches are studied in a scenario where macrocells are sectorized and each sector has at most one outdoor femtocell which acts as a fixed relay. In the direct approach, the original problem of optimizing the tilt angles (so that the aggregate throughput in all femtocells achieves a maximum), is decomposed into a local subproblem consisting of finding the optimum angle when a triplet of closest interferers is considered in each case.

In contrast with the normal approach used when modelling wireless networks via PPP, recent works have moved one step forward towards more realistic models by including the antenna radiation pattern in the calculations. In [17], the authors developed a model to characterize the performance of a HetNet with directional antennas having a 2D radiation pattern. A methodology to characterize the performance of the network in terms of the coverage probability is proposed for a model in which a user is associated with the BS and sector which provides the highest long term (fading being averaged) received power. Moreover, authors analysed the performance of two different antenna patterns and compared the results with the omnidirectional case. In [18], the effect of the beamwidth and orientation error on the coverage and throughput were investigated for a system with directional antennas where transmitters rotate the foresight of their antennas towards the direction of the intended receivers. With the use of stochastic geometry a model was proposed for a network in which transmitters and receivers are located at a fixed distance. A simplification of the directional antenna pattern was made, in which the gains in the main and back lobes are considered to be constant. An extension of directional antennas to millimeter wave cellular networks has been considered in [19], where a line of sight (LOS) probability model was developed as a function of the distance between transmitter and receiver. Coverage and rate expressions are provided for a system where the impact of blockages is taken into account. The simplified model provided considers a fixed gain for the main and back lobes of the antennas, and an approximation of the LOS region as a ball with fixed size. A similar model has been used in [20] where a fixed value for both, the main and back lobes is considered in a millimeter wave system. A new model is proposed by taking into account the channel and blockage empirical models recently reported. Additionally,

a "two ball" approximation is proposed to model the state of the links. The model also accounts for beamforming pointing errors. Expressions for the expected coverage and data rates are provided for two cell association policies, namely, smallest path loss and the highest received power. The impact of the horizontal antenna pattern and blockages in a dense urban cellular network is presented in [21]. The authors quantized the accuracy of the point process model by comparing it with experimental data from an actual deployment of base stations. Additionally, the authors proposed models of both blockages and antenna pattern which result in a tractable analytical framework. Results showed that the point process is suitable for the modelling of future dense urban networks, when the models for blockages and antenna patterns are accurate.

B. Contributions

In contrast to previous works on antenna tilt optimization, we follow a stochastic geometry approach to model the location of the base stations on the network for both, traditional cellular macro network and a HetNet consisting of macro- and femtocells. Employing the well established framework of point processes from stochastic geometry, we can obtain tractable expressions. These expressions can be employed to evaluate the overall performance of the network, without the need to run time consuming simulations, effectively providing a theoretical framework from which the performance of a traditional cellular macro network, and a HetNet can be analysed. Additionally, we address the case of an ultra dense user deployment in which the number of femtocells in the area can vary according to the number of users who purchase them, or through sleep mode scheduling, etc. Therefore, the density of femtocells changes according to the users' needs and it is not a controlled variable, in contrast with scenarios where the tilt is modified in order to serve a particular hotspot. Thus, we can obtain pseudo closed-form expressions with which the scalability of the network can be addressed. It is worthwhile to notice that the results cannot be used in a SON manner, as there is a need to solve the optimization problems formulated. However, these results provide an overall optimum performance in the entire network which could easily be used as a starting point for a SON algorithm or as a tool to adapt to a slowly varying network. The main contributions of this work are as follows.

- *Stochastic approach with full antenna pattern*: Most of the works where stochastic geometry has been used to model the network do not consider an antenna pattern and resort to an omnidirectional antenna assumption. On the other hand, works where an antenna pattern is considered (with the use of stochastic geometry) have traditionally focused on a 2-D horizontal antenna pattern [17]–[21], and make use of a fixed main and back lobe gain. In this work we attempt to create a bridge between these two approaches by proposing a simplistic (yet realistic) model of the 3-D antenna pattern to go along with a stochastic approach for the positioning of the base stations. This is done by taking as baseline the antenna pattern model recommended by 3GPP [22] with some simplifications in the horizontal plane thanks to stochastic geometry properties. On the vertical plane, we make use of the exact antenna patter proposed in [22] which provides an exact characterization. Thus, the analysis is simplified while maintaining a realistic model.
- *Optimum tilt angle for a traditional network*: In contrast to previous works, we focus on the impact of the vertical antenna pattern on the system performance. We derive coverage and EE formulas for the case of a traditional network. In this scenario, the optimum tilt is the one that provides the best performance in terms of the coverage probability and EE. With the resulting expressions, the dependency of the optimum tilt angle on the density of the macrocells is investigated without the need to run time consuming scenario-specific simulations.
- *Optimum tilt angle for a two-tier network when both macro- and femtocells share the same resources*: In this scenario, as it was obtained from simulations, the interference from the femtocell tier to the macrocell users is really high, and so the performance in the macrocell tier is highly deteriorated. Therefore, we propose the use of a guard zone to protect the macrocell user from the femto-tier interference. Then, we formulate an optimization problem to jointly select the optimum antenna tilt angle and guard zone that provide the highest EE of the network when minimum constraints on Quality of Service (QoS) are considered for each tier.

C. Organisation

The outline of this paper is the following. The proposed system model is described in Section II for both the macro and femto tiers. In Section III, we obtain the coverage probability expressions for both macrocells and femtocells. Section IV describes the EE metric used and the optimization problems proposed. In Section V we present the numerical results of this work. Finally, in Section VI, concluding remarks are presented.

The following notation will be used throughput the paper. $E[X]$ stands for the expected value of the random variable X. A random variable X following a complex Gaussian distribution with mean μ and variance σ^2 is expressed as $X \sim \mathcal{CN}(\mu, \sigma^2)$. Finally, a Poisson distribution with mean μ is expressed as Pois (μ), and an exponential distribution with mean μ is written as $\text{Exp}(\frac{1}{\mu})$.

II. System Model

Consider the downlink of a two-tier cellular OFDMA system (such as LTE) consisting of macro- and femtocells, where both share the same resources for transmission, which are assigned as a time-frequency pair. Then in each time slot a user can be served on an available subchannel. We model the base stations in both tiers as independent Poisson Point Processes (PPPs) Φ_i, $i \in \{m, f\}$, where m and f stand respectively, for macro- and femtocell. The number of base stations N_i, follows a Poisson random variable with parameter λ_i, i.e. $N_i \sim \text{Pois}(\lambda_i \mathcal{S})$, $i \in \{m, f\}$, where $\mathcal{S}$ is the deployment area of the network. The base stations are randomly (uniformly) distributed across $\mathcal{S}$. The assumption of femtocells modelled as a PPP follow the

lines of other works [23]–[26] where it is assumed that users acquire their FAPs and place them inside their houses, offices, etc., where an increase in coverage and/or data rates is required. The propagation model is a composite of Rayleigh fading (with $h_{j,i} \sim \mathcal{CN}(0, 1)$ representing the channel between j-th transmitter and i-th receiver) and path loss $l(R) = R^{-\alpha_i}$, dependent on the distance R from transmitter to receiver and the path loss exponent α_i, $i \in \{m, f\}$. Each MBS is assumed to be sectorized with N_s sectors. We assume an ultra dense user scenario where all base stations always have a user to serve and also assume that a symbol $s_{j,k}$, is sent in each time slot, where $E[|s_{j,k}|^2] = 1$. We also assume that all N_s sectors operate in a different subchannel. In the macrocell tier, each user connects to the base station which provides the highest long term expected received power. In other words, the users will be assigned to the closest base station. Under this scheme, the network cells form a Voronoi tesselation [10]. This means that the size (and shape) of the macrocells are variable, in contrast with the typical regular grid shapes commonly used, such as the hexagonal grid. In order to provide a realistic scenario for the sizes of the macrocells, we match the mean area of a Voronoi cell with the area of a hexagonal grid cell, e.g., in a PPP with density value of $\lambda = 1.54 \text{ x } 10^{-6}$ the (mean) Voronoi cell area corresponds to that of a hexagonal shape cell with radius 500 m, approximately. In the case of femtocells, we assume that each FAP has a user to serve and which is located indoors and uniformly distributed in the femtocell coverage area with radius R_f. The FAP radiation pattern is assumed to be omnidirectional in accordance with 3GGP specifications [22]. Also according to LTE specifications, for the MBSs we model the antenna vertical radiation pattern G, which expressed in [27] as

$$G_{dB}(\phi_{tilt}) = -\min\left(12\left(\frac{\phi + \phi_{tilt}}{\phi_{3dB}}\right)^2, A_{dB}\right) \tag{1}$$

where $\phi < 0$ is the angle between the base station antenna and the receiver, $\phi_{tilt} > 0$ is the tilt angle, ϕ_{3dB} represents the 3 dB beamwidth with value 10, and A_{dB} is the minimum power which is leaked to the sectors other than the desired one, and which has a typical value of 20 dB. As for the horizontal plane, we make use of the thinning property of a PPP, and so we thin the PPP by a factor equal to the number of sectors, i.e., we consider an omnidirectional pattern in the horizontal plane, but the effective density of interferers is expressed as $\frac{\lambda}{N_s}$. This assumption is justified given that in the downlink, the radiation pattern of the antennas is symmetric in the horizontal plane, i.e., modifying the pattern of all antennas in the network similarly (as a result of sectorization) does not modify significantly the SIR perceived by the desired user. In addition, as each sector is assumed to operate in a different subchannel, the interference is reduced by a factor of N_s. The angle between the base station antenna and the desired user's antenna ϕ can be expressed as a function of the effective height H_{eff} (difference in heights between transmitter and receiver antenna), and the distance R between the transmitting base station and a receiver, as

$$\phi = -\tan^{-1}\left(\frac{H_{eff}}{R}\right) \tag{2}$$

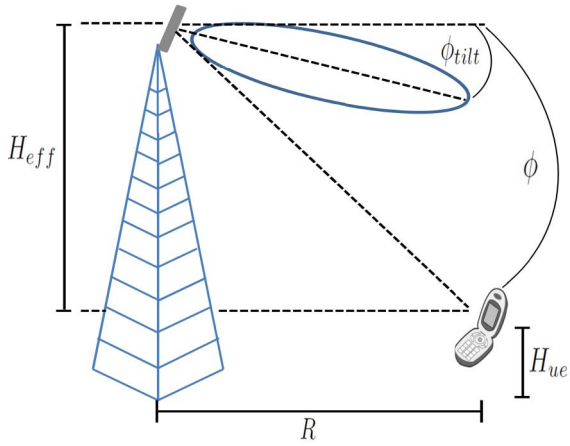

Fig. 1. Vertical antenna pattern and tilt angle.

where $H_{eff} = H_a - H_{ue}$ represents the effective height that results from substracting the user equipment's height H_{ue} from the base station's antenna height H_a. Applying this definition to (1), and converting to linear scale, we obtain

$$G(R, \phi_{tilt}) = 10^{-\min\left(12\left(\frac{-\tan^{-1}\left(\frac{H_{eff}}{R}\right)+\phi_{tilt}}{\phi_{3dB}}\right)^2, A_{dB}\right)/10}. \tag{3}$$

The antenna vertical pattern as well as the tilt angle are depicted in Fig. 1. Now, from the definition of (3) we observe that $G(R, \phi_{tilt})$ can be divided into 2 or 3 parts (depending upon the tilt angle), because of the limiting value of A_{dB}. So, for small values of ϕ_{tilt}, there is only a value of $R = r_{th1}$ at which the function value reaches $-A_{dB}$. However, when ϕ_{tilt} is large enough, there are two values of R (r_{th1} and r_{th2}) at which the function reaches its limit. And so, solving for the threshold distances r_{th1} and r_{th2}, we obtain

$$r_{th1} = \frac{H_{eff}}{\tan\left(\sqrt{A_{\text{dB}}/12}\ \phi_{3dB} + \phi_{tilt}\right)} \tag{4}$$

$$r_{th2} = \frac{H_{eff}}{\tan\left(-\sqrt{A_{\text{dB}}/12}\ \phi_{3dB} + \phi_{tilt}\right)}. \tag{5}$$

Note from Eq. (5) that r_{th2} only takes positive values when the condition $\phi_{tilt} \geq \sqrt{A_{\text{dB}}/12}\ \phi_{3dB}$ is fulfilled, and so, Eq. (3) can be expressed as follows

$$G(R, \phi_{tilt}) = \begin{cases} A & \text{if } R < r_{th1} \\ 10^{-1.2\left(\frac{-\tan^{-1}\left(\frac{H_{eff}}{R}\right)+\phi_{tilt}}{\phi_{3dB}}\right)^2} & \text{if } R \geq r_{th1} \end{cases} \tag{6}$$

for $\phi_{tilt} < \sqrt{A_{dB}/12}\ \phi_{3dB}$, and

$$G(R, \phi_{tilt}) = \begin{cases} A & \text{if } R < r_{th1} \\ 10^{-1.2\left(\frac{-\tan^{-1}\left(\frac{H_{eff}}{R}\right)+\phi_{tilt}}{\phi_{3dB}}\right)^2} & \text{if } r_{th1} \leq R < r_{th2} \\ A & \text{if } R \geq r_{th2} \end{cases} \tag{7}$$

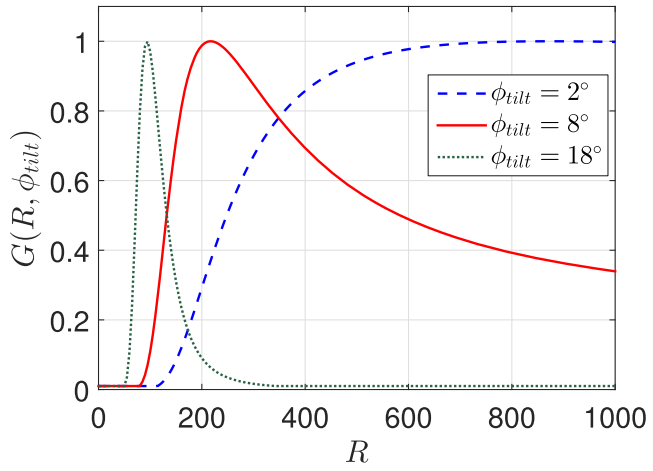

Fig. 2. Vertical antenna pattern (3), as a function of the distance R from base station to the user for antenna tilt values $\phi_{tilt} = 2°, 8°$ and $18°$. Note that depending on the tilt angle, the shape of the lines change and the function can be further defined by parts as in (6) or (7).

for $\phi_{tilt} \geq \sqrt{A_{dB}/12}\ \phi_{3dB}$, where A is the value of $-A_{dB}$ in linear scale. The vertical antenna pattern, re-defined in terms of the distance from the MBS to the user, is presented in Fig. 2 for values of antenna tilt $\phi_{tilt} = 2°, 8°$ and $18°$. Note that the maximum angle between the user and the MBS is $0°$, when $R \to \infty$, and so the horizontal axis sets a limit on the values that the function $G(R, \phi_{tilt})$ can take. Therefore, it can be seen that when the antenna tilt is small ($\phi_{tilt} < \sqrt{A_{dB}/12}\ \phi_{3dB}$) the function is defined by 2 parts as in (6) because the function $G(R, \phi_{tilt})$ never reaches the value A as R increases. However, as the tilt angle becomes large enough ($\phi_{tilt} \geq \sqrt{A_{dB}/12}\ \phi_{3dB}$), the function is now defined by 3 parts as in (7) due to the fact that for a given value of R the function does attain value A.

III. Coverage

In this section, we obtain the coverage probability expressions first for a traditional network (macrocells only) and then for a HetNet consisting of femtocells overlaid with the macrocell tier. We consider an interference limited scenario, and so the effect of noise will be neglected. However, it could be easily included into the calculations in a straightforward manner.

A. Traditional Macrocell Network

For a macrocell traditional network, there is one PPP Φ_m used to model the positions of the MBSs. Considering that the user connects to the closest MBS, the received signal at the user in a given time slot is expressed as

$$y = \sqrt{P_m^{tx}\ l\left(r_{0,0}\right) G(r_{0,0}, \phi_{tilt})}\ h_{0,0}\, s_{0,0} + \sum_{j \in \Phi_m \setminus \{0\}} \sqrt{P_m^{tx}\ l\left(r_{j,0}\right) G(r_{j,0}, \phi_{tilt})}\ h_{j,0}\, s_{j,j} \quad (8)$$

where P_m^{tx} is the MBS transmit power, $r_{j,k}$, $h_{j,k}$ and $s_{j,k}$ are respectively, the distance, channel gain and symbol sent from the j-th base station to the k-th user. Note that $r_{0,0}$ represents the distance from the closest base station to the desired user. For easiness of representation we drop the subscripts in the desired link. Using Slivnyak's theorem [28], placing a typical point at the origin does not change the statistics of the PPP, and so we locate the typical user at the origin and obtain its statistics. The signal to interference ratio (SIR) is given by

$$SIR = \frac{|h|^2\, r^{-\alpha}\, G(r, \phi_{tilt})}{\sum_{j \in \Phi_m \setminus \{0\}} |h_{j,0}|^2\, r_{j,0}^{-\alpha}\, G(r_{j,0}, \phi_{tilt})} = \frac{|h|^2\, r^{-\alpha}\, G(r, \phi_{tilt})}{I_{\Phi_m}} \quad (9)$$

where I_{Φ_m} is the effective interference from the base stations and $|h_{j,k}|^2 \sim \text{Exp}(1)$. The coverage probability P^c is defined as the probability that the received SIR in the entire service area is above a certain threshold β, which depends on the network's Quality of Service (QoS). From (9), we have

$$\begin{aligned} P^c &= P(SIR > \beta) \\ &= E_{r, I_{\Phi_m}}\left[\exp\left(-s\, I_{\Phi_m}\right)\right]|_{s=\beta r^\alpha\, G(r,\phi_{tilt})} \\ &= E_r\left[E_{I_{\Phi_m}}\left[\exp\left(-s\, I_{\Phi_m}\right)\right]\right] \\ &= E_r\left[\mathcal{L}_{I_{\Phi_m}}(s)\right] \end{aligned} \quad (10)$$

where $\mathcal{L}_{I_{\Phi_m}}(s)$ is the Laplace transform of the interference I_{Φ_m}, and the expectation with respect to r is obtained using the fact that the distance to the closest base station for a PPP is Rayleigh distributed [10], i.e. $f(r) = 2\pi\lambda r\, e^{-\lambda\pi r^2}$. The value of the Laplace transform is expressed as

$$\begin{aligned} \mathcal{L}_{I_{\Phi_m}}(s) &= E_{\Phi_m, |h_{j,0}|^2}\left[e^{-s \sum\limits_{j \in \Phi_m} |h_{j,0}|^2\, r_{j,0}^{-\alpha}\, G(r_{j,0}, \phi_{tilt})}\right] \\ &= E_{\Phi_m}\left[\prod_{j \in \Phi_m} E_{|h_{j,0}|^2}\left[e^{-s\,|h_{j,0}|^2\, r_{j,0}^{-\alpha}\, G(r_{j,0}, \phi_{tilt})}\right]\right]. \end{aligned} \quad (11)$$

Given the fact that $|h_{j,0}|^2$ is independent for all $j \in \Phi_m$ and $|h_{j,0}|^2 \sim \text{Exp}(1)$, by taking the inner expectation in (11), we obtain

$$\mathcal{L}_{I_{\Phi_m}}(s) = E_{\Phi_m}\left[\prod_{j \in \Phi_m} \left(1 + s\, r_{j,0}^{-\alpha}\, G\left(r_{j,0}, \phi_{tilt}\right)\right)^{-1}\right]. \quad (12)$$

Using the definition of the generating functional of a PPP [28] we obtain

$$\begin{aligned} \mathcal{L}_{I_{\Phi_m}}(s) &= \exp\left(-\frac{2\pi\lambda_m}{Ns}\int_r^\infty \frac{y\ \mathrm{d}y}{1 + s^{-1}\, y^{\alpha_m}\, G^{-1}(y, \phi_{tilt})}\right) \\ &= \exp\left(-\frac{2\pi\lambda_m}{Ns}\int_r^\infty \frac{y\ \mathrm{d}y}{1 + \left(\frac{y}{r}\right)^{\alpha_m} \frac{G^{-1}(y,\phi_{tilt})}{\beta\, G^{-1}(r,\phi_{tilt})}}\right). \end{aligned} \quad (13)$$

Substituting (13) into (10), and using the definitions in (6) and (7), the coverage probability can be expressed as in (15), shown at the top of the next page, where $\zeta(a, b) = {}_2F_1(1, 1 - \frac{2}{a};$

$$P^c = \begin{cases} \int_0^{r_{th1}} 2\lambda_m \pi r \ \mathrm{e}^{-\lambda_m \pi \left\{ r^2 + \frac{2}{Ns}\left[\frac{\beta r^{\alpha_m}}{\alpha_m - 2}\left(r^{-\alpha_m - 2}\,\zeta_1 - r_{th1}^{-\alpha_m+2}\,\zeta_2 \right) + \rho_1 \right] \right\}} \, dr + \int_{r_{th1}}^{\infty} 2\lambda_m \pi r \ \mathrm{e}^{-\lambda_m \pi \left\{ r^2 + \frac{2}{Ns}\rho_2 \right\}} \, dr \\ \text{if } \phi_{tilt} < \sqrt{\frac{A_{dB}}{12}} \ \phi_{3dB} \\ \int_0^{r_{th1}} 2\lambda_m \pi r \ \mathrm{e}^{-\lambda_m \pi \left\{ r^2 + \frac{2}{Ns}\left[\frac{\beta r_m^{\alpha}}{\alpha_m - 2}\left(r^{-\alpha_m + 2}\,\zeta_1 - r_{th1}^{-\alpha_m+2}\,\zeta_2 \right) + r_{th2}^{-\alpha_m+2}\zeta_3 + \rho_3 \right] \right\}} \, dr \\ + \int_{r_{th1}}^{r_{th2}} 2\lambda_m \pi r \ \mathrm{e}^{-\lambda_m \pi \left\{ r^2 + \frac{2}{Ns}\left[\rho_4 + \frac{\beta A F^{-1}(r,\phi_{tilt})\, r^{\alpha_m} r_{th2}^{-\alpha_m+2}}{(\alpha_m - 2)}\,\zeta_4 \right] \right\}} \, dr + \frac{\exp\left(-\lambda_m \pi r_{th2}^2 \left\{ 1 + \frac{2}{Ns}\left[\frac{\beta}{\alpha_m - 2}\,\zeta_1 \right] \right\} \right)}{1 + \frac{2}{Ns}\left(\frac{\beta}{\alpha_m - 2}\zeta_1 \right)} \\ \text{if } \phi_{tilt} \geq \sqrt{\frac{A_{dB}}{12}} \ \phi_{3dB} \end{cases} \tag{15}$$

with $\zeta_1 = \zeta(\alpha_m, \beta)$, $\zeta_2 = \zeta(\alpha_m, (\frac{r_{th1}}{r})^{-\alpha_m}\beta)$, $\zeta_3 = \zeta(\alpha_m, (\frac{r_{th2}}{r})^{-\alpha_m}\beta)$, $\zeta_4 = \zeta(\alpha_m, (\frac{r_{th2}}{r})^{-\alpha_m}\beta A F^{-1}(r, \phi_{tilt}))$, $\rho_1 = \rho(r_{th1}, \infty, \frac{AF^{-1}(y,\phi_{tilt})}{\beta})$, $\rho_2 = \rho(r, \infty, \frac{F^{-1}(y,\phi_{tilt})}{\beta\, F^{-1}(r,\phi_{tilt})})$, $\rho_3 = \rho(r_{th1}, r_{th2}, \frac{AF^{-1}(y,\phi_{tilt})}{\beta})$, $\rho_4 = \rho(r, r_{th2}, \frac{F^{-1}(y,\phi_{tilt})}{\beta\, F^{-1}(r,\phi_{tilt})})$.

$2 - \frac{2}{a}; -b)$ is the Gauss hypergeometric function, $\rho\,(a, b, c) = \int_a^b \frac{y\, dy}{1 + (\frac{y}{r})^{\alpha_m} c}$, and we made use of the following function definition

$$F(a, \phi_{tilt}) = 10^{-1.2\left(\frac{-\tan^{-1}\left(\frac{H_{eff}}{a} \right) + \phi_{tilt}}{\phi_{3dB}} \right)^2}. \tag{14}$$

The derivation of (15) is found in Appendix A.

B. Heterogeneous Network

We now consider the case of a HetNet consisting of macro- and femtocells deployed in the coverage area. The femtocells are assumed to operate in closed subscriber group, meaning that they only serve their subscribed users which are assumed to be located indoors. As mentioned in section II, the antennas of the FAPs are all assumed to have an omnidirectional pattern [22]. The FAPs are also assumed to operate in the same frequencies as the macrocells. Therefore, there is inter-tier interference from macro- to femtocells and vice-versa. As previously stated, the femtocell users are uniformly distributed in the coverage area of their serving FAP, which corresponds to a circular area of radius R_f. A wall partition loss L_w, defined as the amount of power which is lost when the signal goes through a wall, is considered also.

Now, as the macrocell users are seriously affected by the femtocell tier interference, we propose the use of a guard zone with radius R_c protecting the macrocell users from the nearby FAPs interference. In this scenario, a cooperation is assumed between femto and macro tiers, where if femtocells detect a macrocell user within a distance R_c, they will restrain themselves from transmitting. This assumption is supported by considering that both macro and femtocells are deployed by the same network operator, which can have an estimate on the location of their macrocell users. This information in turn, can be made available to femtocells by means of a macro to femto interface, such as the X2 interface. This model is then equivalent to having a macrocell user with a guard zone preventing any femtocell transmissions within a distance R_c. The potential use of a guard zone has been reported previously to protect a given user from interference [8], [29]. So, with this model we analyse the effect of the guard zone and the tilt angle when changes in the density of femtocells are perceived. Once again, we place the typical users at the origin and then, the received signals by a macrocell user (y_m) and femtocell user (y_f) are given by

$$\begin{aligned} y_m =& \sqrt{P_m^{tx}\, l\left(r_{0,0}\right) G(r_{0,0}, \phi_{tilt})}\ h_{0,0}\, s_{0,0} \\ &+ \sum_{j \in \Phi_m \setminus \{0\}} \sqrt{P_m^{tx}\ l\left(r_{j,0}\right) G(r_{j,0}, \phi_{tilt})}\ h_{j,0}\, s_{j,j} \\ &+ \sum_{k \in \Phi'_f \setminus \{\mathcal{B}(0,R_c)\}} \sqrt{P_f^{tx}\ l\left(d_{k,0}\right) L_w}\ g_{k,0}\, x_{k,k} \end{aligned} \tag{16}$$

$$\begin{aligned} y_f =& \sqrt{P_f^{tx}\, l\left(d_{0,0}\right)}\ g_{0,0}\, x_{0,0} \\ &+ \sum_{j \in \Phi_m} \sqrt{P_m^{tx}\ l\left(r_{j,0}\right) G(r_{j,0}, \phi_{tilt}) L_w}\ h_{j,0}\, s_{j,j} \\ &+ \sum_{k \in \Phi'_f \setminus \{0\}} \sqrt{P_f^{tx}\ l\left(d_{k,0}\right) L_w^2}\ g_{k,0}\, x_{k,k} \end{aligned} \tag{17}$$

where $\mathcal{B}(x, b)$ represents the 2-dimensional ball with radius b centered at x, P_m^{tx} (P_f^{tx}) is the transmission power of a MBS(FAP), $r_{j,k}$ ($d_{j,k}$) is the distance from the j-th MBS (FAP) to the k-th user, $h_{j,k}$ ($g_{j,k}$) is the Rayleigh fading channel between the j-th MBS (FAP) and the k-th user and $s_{j,k}$ ($x_{j,k}$) is the transmitted symbol from the j-th MBS (FAP) to the k-th user, with $|s_{j,k}|^2 = 1$ ($|x_{j,k}|^2 = 1$). Additionally, Φ'_f represents the femtocell resulting point process after all FAPs that fall within the guard zone of a macrocell user have been removed in each macrocell. Note that in the femtocell tier, we use L_w^2 given the assumption that femtocell users are located indoors, and so the interfering signal has to get throught two walls. For easiness of representation, from now on we drop the subscript in the desired links. The SIRs are given as

$$SIR_m = \frac{|h|^2\, r^{-\alpha_m}\, G\,(r, \phi_{tilt})}{I_{\Phi_m}^m + I_{\Phi'_f}^m} \tag{18}$$

$$SIR_f = \frac{|g|^2\, d^{-\alpha_f}}{I_{\Phi_m}^f + I_{\Phi'_f}^f} \tag{19}$$

where $I^m_{\Phi_m} = \sum_{j\in\Phi_m\setminus\{0\}} |h_{j,0}|^2\, r_{j,0}^{-\alpha_m}\, G(r_{j,0},\phi_{tilt})$ and $I^m_{\Phi'_f} = \sum_{k\in\Phi'_f\setminus\{\mathcal{B}(0,R_c)\}} |g_{j,0}|^2 \eta\; d_{k,0}^{-\alpha_f} L_w$, represent, respectively, the interference from the macrocell and femtocell tier observed by the macrocell user. Additionally, $I^f_{\Phi_m} = \sum_{j\in\Phi_m} |h_{j,0}|^2\, r_{j,0}^{-\alpha_m}\, G(r_{j,0},\phi_{tilt})$ and $I^f_{\Phi'_f} = \sum_{k\in\Phi'_f\setminus\{0\}} |g_{k,0}|^2\, d_{k,0}^{-\alpha} L_w^2$ represent, respectively, the interference from the macrocell and femtocell tier perceived by the femtocell user. Following the same approach as for the traditional network, the coverage probability in the macrocell tier is given as

$$\begin{aligned} P^c_m &= P(SIR_m > \beta_m) \\ &= E_{r, I^m_{\Phi_m}, I^m_{\Phi'_f}} \left[\exp\left(-s\, I^m_{\Phi_m}\right) \exp\left(-\eta L_w s\, I^m_{\Phi'_f}\right) \right] \\ &= E_r \left[E_{I^m_{\Phi_m}} \left[\exp\left(-s\, I^m_{\Phi_m}\right) \right] E_{I^m_{\Phi'_f}} \left[\exp\left(-\eta L_w s\, I^m_{\Phi'_f}\right) \right] \right] \\ &= E_r \left[\mathcal{L}_{I^m_{\Phi_m}}(s)\, \mathcal{L}_{I^m_{\Phi'_f}}(\eta L_w s) \right] \end{aligned} \tag{20}$$

where $s = \beta_m r_m^{\alpha}\, G(r,\phi_{tilt})$ and $\eta = \frac{P^{tx}_f}{P^{tx}_m}$. The Laplace transform of the macrocell tier can be expressed as

$$\mathcal{L}_{I^m_{\Phi_m}}(s) = \exp\left(-\frac{2\pi\lambda_m}{Ns} \int_r^{\infty} \frac{y\ \mathrm{d}y}{1 + \left(\frac{y}{r}\right)^{\alpha_m} \frac{F^{-1}(y,\phi_{tilt})}{\beta_m\, F^{-1}(r,\phi_{tilt})}} \right). \tag{21}$$

where the definition of the generating functional of a PPP was again used. It is worthwhile to notice that we have approximated (3) by (14) in this case. This approximation was not used in section III-A, because a macrocell only network, not providing a minimum radiated power (A_{dB}), results in not considering the minimum amount of interference leaked, which in turn is reflected in the optimum tilt angle always taking the maximum allowable value. In the case of the HetNet, this assumption is possible, since the femtocell tier provides the baseline interference. Note also that the Laplace transform for the macrocell interference I_{Φ_m} can be neglected in some scenarios where a large number of femtocells are deployed in the area. This depends on the values of the wall partition loss and path loss exponent. This assumption can greatly simplify the analysis (and speed up the result of the proposed optimization)

On the other hand, the Laplace transform of the interference from femtocells to macrocells ($L^m_{\Phi'_f}$) forms a hole point process for which an approximation (lower bound) can be expressed by considering the interference outside R_c and using the formula for Rayleigh fading in [30]. The Laplace transform is then given by

$$\mathcal{L}_{I^m_{\Phi'_f}}(\eta L_w s) = e^{-\lambda_f \pi \left((\eta L_w s)^{\delta_f} E_h\left[h^{\delta_f} \gamma\left(1-\delta_f, \eta L_w s h R_c^{-\alpha_f}\right)\right] - \frac{R_c^2 \eta s}{\eta L_w s + R_c^{\alpha_f}} \right)}. \tag{22}$$

where $h \sim \mathrm{Exp}(1)$. We further extend (22) and express $\mathcal{L}_{I_{\Phi'_f}}$ as

$$\begin{aligned} \mathcal{L}_{I^m_{\Phi'_f}}(\eta L_w s) &= e^{\lambda_f \pi R_c^2} \\ &\quad \cdot e^{-\lambda_f \pi R_c^2\, {}_2F_1\left(1,-\delta_f;1-\delta_f;-\beta r^{\alpha_m} F^{-1}(r)\eta L_w R_c^{-\alpha_f}\right)}. \end{aligned} \tag{23}$$

The derivation of (23) is given in Appendix B. Then, using the expressions for the Laplace transforms found in (21) and (23), the coverage probability for the macrocell tier is expresed as in (28), which is shown at the top of p. 8, where $C(\alpha_m,\phi_{tilt},r) = \int_r^{\infty} \frac{y\ \mathrm{d}y}{1+\left(\frac{y}{r}\right)^{\alpha_m} \frac{F^{-1}(y,\phi_{tilt})}{\beta_m\, F^{-1}(r,\phi_{tilt})}}$.

In the case of the femtocell tier, the number of femtocells which are interfering with each other is reduced due to the fact that all the femtocells which fall within the area comprised within a radius of R_c surrounding a macrocell user will not transmit. Therefore, we use the thinning property of a PPP [28], in which case the effective density of interfering femtocells is given by $p\lambda_f$, where p is the thinning probability. Consider $\mathcal{V} = \bigcup_{j\in\Phi_m} \mathcal{V}_j$ as the set of all Voronoi cells formed from the PPP Φ_m, where $\mathcal{V}_j$ represents the Voronoi cell having point $x_j \in \Phi_m$ as seed. The thinning probability represents the probability that a femtocell placed at a point $x_k \in \Phi_f$ is located inside a Voronoi cell $\mathcal{V}_j$ and outside the area with radius R_c surrounding a macrocell user located at a point x_u uniformly distributed inside V_j. This applies to all the Voronoi cells in the network as we consider that all cells have a user to serve in each time slot. Thus, the thinning probability can be expressed as

$$\begin{aligned} p &= P\left(x_k \notin \mathcal{B}(x_u, R_c) \mid x_k \in \mathcal{V}_j\right),\ \forall j \in \Phi_m \\ &= 1 - P\left(x_k \in \mathcal{B}(x_u, R_c) \mid x_k \in \mathcal{V}_j\right) \\ &\overset{(a)}{\approx} 1 - \frac{\pi R_c^2}{A_{cell}} \\ &= 1 - \lambda_m \pi R_c^2 \end{aligned} \tag{24}$$

where A_{cell} is the typical (mean) area of a Voronoi cell, which is by definition $A_{cell} = \frac{1}{\lambda_m}$. Note that the approximation in step (a) is obtained by using the ratio of the circular area covered by a radius R_c and the area of the Voronoi cell. Note also from (24), that the maximum radius permissible is $R_c^{max} = \frac{1}{\sqrt{\lambda_m \pi}}$. With this value the area covered by the guard zone equals the mean value of the Voronoi cells. Now, because a femtocell will only transmit if it is outside a radius R_c from a macrocell user, there can be two types of outage: the first is the one that occurs when a femtocell does not transmit (with probability $1-p$) and second is one that takes place when the femtocell does transmit (with probability p) but the perceived SIR_f at the femtocell user is below β_f. Taking this into account, we obtain the mean coverage probability for the femtocell tier as

$$\begin{aligned} P^c_f &= p\, P(SIR_f > \beta_f) \\ &= (1-\lambda_m \pi R_c^2)\, E_d \left[E_{I^f_{\Phi_m}} \left[\exp\left(-s'\eta^{-1} d^{\alpha_0}\, I^f_{\Phi_m}\right) \right] \right. \\ &\qquad \left. E_{I^f_{\Phi'_f}} \left[\exp\left(-s' L_w d^{\alpha_0}\, I^f_{\Phi_f}\right) \right] \right] \\ &= (1-\lambda_m \pi R_c^2)\, E_d \left[\mathcal{L}_{I^f_{\Phi_m}}(s'\eta^{-1} d^{\alpha_0})\, \mathcal{L}_{I^f_{\Phi'_f}}(s' L_w d^{\alpha_0}) \right]. \end{aligned} \tag{25}$$

$$P_m^c = \mathrm{e}^{\lambda_f \pi R_c^2} \int_0^\infty 2\lambda_m \pi r \, \mathrm{e}^{-\lambda_m \pi r^2 \left(1+\frac{2}{r^2 N_s} C(\alpha_m, \phi_{tilt}, r)\right) - \lambda_f \pi R_c^2 \, {}_2F_1\left(1, -\frac{2}{\alpha_f}; 1-\frac{2}{\alpha_f}; -\beta r^{\alpha_m} F(r,\phi_{tilt})^{-1} \eta L_w R_c^{-\alpha_f}\right)} dr \tag{28}$$

$$P_f^c = \left(1 - \lambda_m \pi R_c^2\right) e^{-\lambda_f \left(1-\lambda_m \pi R_c^2\right)\left(\bar{R_f}^{\alpha_0} \beta L_w^2\right)^{\delta_f} \frac{\pi^2 \delta_f}{\sin(\pi \delta_f)} - \frac{2\pi\lambda_m}{N_s} \int_0^\infty \frac{x\, dx}{1+\beta^{-1} \bar{R_f}^{-\alpha_0} F^{-1}(x,\phi_{tilt}) x^{\alpha_m}}} \tag{29}$$

where $s' = \beta_f L_w$. In order to simplify the analysis, and thanks to the small expected distances between femtocells users and their serving FAPs, we use Jensen's inequality in (25), in which case the femtocell coverage probability is approximated by

$$P_f^c \approx \left(1 - \lambda_m \pi R_c^2\right) \mathcal{L}_{I_{\Phi_m}^f}\left(s' \eta^{-1} \bar{R_f}^{\alpha_0}\right) \mathcal{L}_{I_{\Phi'_f}^f}\left(s' L_w \bar{R_f}^{\alpha_0}\right) \tag{26}$$

where $\bar{R}_f = \frac{2R_f}{3}$, is the expected value of the distance from femtocell users to their designated FAP. This expected value was found using the fact that the pdf of the distance D to the origin of a user uniformly distributed in a circular area of radius R_f is $f_D(d) = \frac{2d}{R_f^2}$ [24]. The results of simulations presented in section V show that this approximation is indeed very accurate. Using the definition of the generating functional of a PPP like in the macrocell only case, the Laplace transform of the macrocell interference can be expressed as

$$\mathcal{L}_{I_{\Phi_m}^f}\left(s' \eta^{-1} \bar{R_f}^{\alpha_0}\right) = e^{-\frac{2\pi\lambda_m}{N_s} \int_0^\infty \frac{x\, dx}{1+\beta^{-1} \bar{R_f}^{-\alpha_0} F^{-1}(x,\phi_{tilt}) x^{\alpha_m}}}. \tag{27}$$

On the other hand, the Laplace transform $\mathcal{L}_{I_{\Phi'_f}^f}(s' L_w \bar{R_f}^{\alpha_0})$ in (25) can be obtained directly from [31], considering the reduction of the interfering femtocells by a factor p. Therefore, using the values for the Laplace transforms previously described, the femtocell tier coverage probability is given as in (29), shown at the top of the page. As in the macrocell coverage probability, for a highly dense scenario and depending on the wall partition loss, the interference from the macrocell tier could be neglected, resulting in a closed form expression for the femtocell coverage probability for those particular scenarios.

IV. Energy Efficiency

We use the inverse of the Energy Consumption Rating (ECR) to characterize the EE of the network, which is given by

$$EE = \frac{T}{P} \quad \text{b/J/Hz} \tag{30}$$

where T is the achievable throughput in bps/Hz and P is the total power consumed in Watts. So, the EE for the traditional and heterogeneous networks is given by

$$EE = \frac{\sum_{i \in \{m,f\}} \lambda_i P_i^c \log_2(1+\beta_i)}{\sum_{i \in \{m,f\}} \lambda_i P_i^T} \tag{31}$$

where P_i^T is the total power consumed by a base station in the i-th tier. For P_i^T, we make use of the commonly used model [32]–[34], which for macro- and femtocells is given by

$$P_m^T = N_s \left(P_{cm} + \kappa_m P_m^{tx}\right) \tag{32}$$

$$P_f^T = P_{cf} + \kappa_f P_f^{tx} \tag{33}$$

where P_i^{tx} is the transmit power in the i-th tier, P_{ci} is the constant power component related to the signal processing, cooling of the site as well as battery backup in the i-th tier and κ_i is a factor related to the efficiency of the power amplifier in the i-th tier. The power related component values, along with the other network's parameters are presented in Table I. We proceed to define the EE optimizations for both the traditional and two-tier networks.

A. Traditional Macrocell Network

For the case of an traditional network, the expression in (31) is simplified and the optimization problem proposed consists of finding the optimum antenna tilt (ϕ_{tilt}^*) that maximizes the EE of the network, i.e.

$$\phi_{tilt}^* = \arg\max_{\phi_{tilt}} \underbrace{\frac{P_m^c(\beta_m, \phi_{tilt}) \log_2(1+\beta_m)}{N_s\left(P_{cm} + \kappa_m P_m^{tx}\right)}}_{EE}. \tag{34}$$

Due to the complexity of the expression for EE in (34), we cannot find a closed-form solution. However, as the tilt angle is limited (same as its sensitivity in practice), the solution can be found for a small number of steps using a greedy search over the possible tilt values. Therefore, the complexity of the algorithm is simply $n_{degrees}$, where $n_{degrees}$ is the number of possible antenna tilts that the RET can provide. The results obtained for the traditional network are found in Section V.

B. Heterogeneous Network

In the case of the two-tier network described in Section III, the guard zone R_c has the effect of enhancing the performance of the macrocell tier by reducing the received interference from femtocells located in the vicinity of a macrocell user, therefore a bigger value of R_c is desired in this case. However, the selection of the size of R_c has a negative impact in the femtocell tier, given the fact that increasing its size would cause a higher number of femtocells to stop transmitting, and so, the coverage probability in this tier would be reduced. This leads to the conclusion that there must be a tradeoff in the selection of the guard zone size to balance the performance of macro- and femtocell tiers. On the other hand, as described in Section I, the selection of the tilt angle ϕ_{tilt} can significantly increase the performance of the macrocell tier, and with the inclusion of a tier of interfering femtocells its optimum value is different from the one found for a traditional network. Furthermore,

TABLE I
SIMULATION PARAMETERS

Parameter	Value	Description
ϕ_{3dB}	10	Half Beamwidth
H_a	32 m	Base station antenna height
H_{ue}	1.5 m	User equipment antenna height
R_f	30 m	Femtocell radius
α_m	3,4	Path loss exponent for the macrocell tier
α_0	2.5, 3	Path loss exponent for the femtocell tier in the desired link
α_f	3,4	Path loss exponent for the femtocell tier in an interference link
L_w	5, 10, 20 dB	Wall partition loss for the femtocell tier
N_s	3, 6	Number of antenna sectors for the macrocell tier
P_f^{tx}	100 mW	Femtocell transmission power
P_m^{tx}	20 W	Macrocell transmission power
κ_f	4	Femtocell power component dependent of the transmission power
κ_m	3.77	Macrocell power component dependent of the transmission power
P_{cf}	9.6	Femtocell constant power component related to signal processing, site cooling, battery backup
P_{cm}	68.73	Macrocell constant power component related to signal processing, site cooling, battery backup

we are interested in obtaining the values of R_c and ϕ_{tilt} that would yield a good performance in terms of the overall network energy efficiency. Taking into account the considerations just described, we propose an optimization problem to maximize the energy efficiency of the network with constraints on the QoS requirements of both tiers. We aim to find both the optimum antenna tilt angle ϕ^*_{tilt} and guard zone R^*_c that maximize the energy efficiency with the required constraints. Formally, the problem is described as follows

$$\phi^*_{tilt}, R^*_c = \arg\max_{\phi_{tilt}, R_c} \underbrace{\frac{\lambda_m P_m^c \log_2(1+\beta_{\mathrm{m}}) + \lambda_f P_f^c \log_2(1+\beta_{\mathrm{f}})}{N_s\left(P_{cm} + \kappa_m P_m^{tx}\right) + P_{cf} + \kappa_f P_f^{tx}}}_{EE}$$
$$\text{s.t.} \quad P_m^c \geq 1-\epsilon_m, \quad P_f^c \geq 1-\epsilon_f \tag{35}$$

where ϵ_m and ϵ_f are respectively, the maximum outage probabilities permitted for macro and femto tiers. We denote $EE^\star$ as the maximum energy efficiency that can be achieved by selecting the optimum values $\phi^\star_{tilt}$ and $R^\star_c$. Although the proposed optimization problem cannot adapt to the changes in the environment in an online fashion, it can still provide an overall solution to the system without the need to run time consuming simulations. Therefore, when a change in the system parameters (such as the densities of macro- and/or femtocell) occurs, the network operators can obtain a centralized solution that will yield a good performance depending upon the changes in the system. For the expressions in (35), we proceed to use a non-linear software package in Matlab, using an interior point method to solve the optimization problem. The numerical results are showed in Section V.

V. RESULTS

The numerical results of this work are presented in figures 3 to 9, where the lines correspond to the analytical results while the circles represent the results of MonteCarlo simulations. The system parameters used in the simulations are presented in Table I, where we have used typical values found in practice. For the simulations, we first generate a random number of MBSs in the area following a PPP. Then, we proceed to obtain the Voronoi tessellation with the MBSs deployed. The typical user is located at the origin and associated with the closest MBS, according to Slivnyak's theorem. Then, we obtain the interference from the other MBSs considering the distant-dependent vertical pattern, while at the same time, the number of interferers is reduced randomly by a factor equal to N_s (number of sectors). In the case of the simulations for the HetNet, the two independent tiers are generated and the same process previously described is used to create the Voronoi cells. Next, in all the Voronoi cells of the network, a randomly (uniformly) distributed user is generated within the area of each Voronoi cell. Then, a circular area of radius R_c is considered around each user and all the FAPs that fall within its circular area are considered inactive. The performance of both macro- and femtocell users is obtained by considering only the femtocells which remain active. Additionally, the simulations for the femtocell tier are obtained by considering that the user is uniformly distributed in the coverage area of its serving FAP, while the analytical results are attained by using the expected value of the distance from the user to its serving FAP, as presented in the theoretical analysis. As mentioned before, we focused on a RET system, where the downtilt of the antenna can be remotely configured. Typical ranges for the electrical antenna tilt found in practice are $0-15°$ [35], [36]. However, state of the art antennas have been reported to achieve $18°$ [37], and even $20°$ [38].

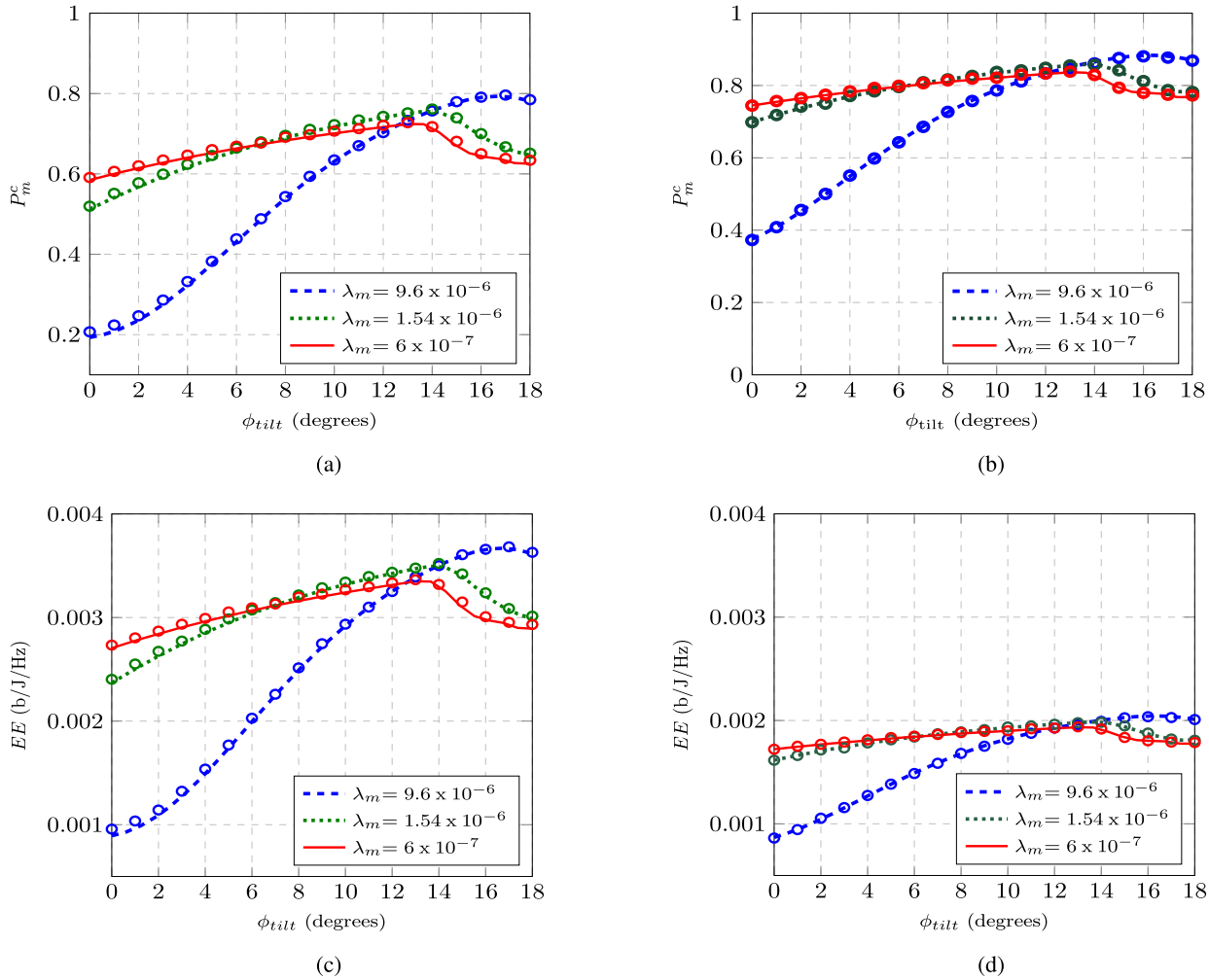

Fig. 3. Coverage probabilities for (a) 3 sectors ($N_s = 3$) and (b) 6 sectors ($N_s = 6$), and energy efficiencies for (c) 3 sectors ($N_s = 3$) and (d) 6 sectors ($N_s = 6$) of a traditional network as a function of ϕ_{tilt},. In all figures, $\beta_m = 3$ and we present the results for $\lambda_m = 9.6 \times 10^{-6}$, 1.54×10^{-6} and 6×10^{-7}.

Therefore we select the latter as the maximum permissible tilt angle in our setup.

The coverage probability and EE of a traditional network are presented in Fig. 3 as a function of the tilt angle. Figures 3(a) and 3(b) show the coverage probabilities for antennas with 120° ($N_S = 3$) and 60° ($N_S = 6$) sectorization, respectively. It can be seen that there is an antenna tilt angle that maximizes the coverage probability (and therefore, the energy efficiency). The former can be explained as follows: for low values of ϕ_{tilt} the coverage probability is low, due to the fact that the direction of the main lobe of the antenna does not point to the desired coverage area of each cell. As ϕ_{tilt} increases, most of the radiated power is pointed towards the area of the desired cell and less interference is created at the neighbouring cells, which is reflected in an increase in the coverage (and energy efficiency) of the network. Finally, the coverage reaches a maximum at the point where a significant portion of the radiated power is projected towards the desired cell while little interference is caused at the other cells. After that maximum, increasing ϕ_{tilt} cause very little interference but would also cover a very small portion of the desired cell, which would make the coverage probability drop. Additionally, it can be seen that (as expected) the optimum tilt angle is strongly coupled with the density of macro stations. This is due to the fact that with a higher density, the mean area of the cells is smaller and so a higher value of the antenna tilt is required to point to the smaller cell area. As is expected, the coverage probability is further increased with the use of more antenna sectors, as the interference is further reduced. On the other hand, Figures 3(c) and 3(d) show the performance in terms of the EE. It can be seen that while the lines follow the same trends as in the case of coverage probability, the 120° sectorized antennas outperform the 60° sectorized antennas. This is due to the fact that the power consumed by using extra antenna sectors has more impact on the EE than the gains in throughput. Therefore, an inherent trade-off between the throughput and the EE of the system can be perceived.

In Fig. 4 the coverage probability for the macrocell and femtocell tiers are shown as a function of the antenna tilt angle and guard zone, respectively. The results are presented for an average number of femtocells 20, 50 and 100 deployed per macrocell, and for different values of path loss exponents and wall partition loss. In 4(a), the coverage probability of the macrocell tier is displayed as a function of the antenna tilt angle when a guard zone of $R_c = 200$ m. is used. It can be seen that the

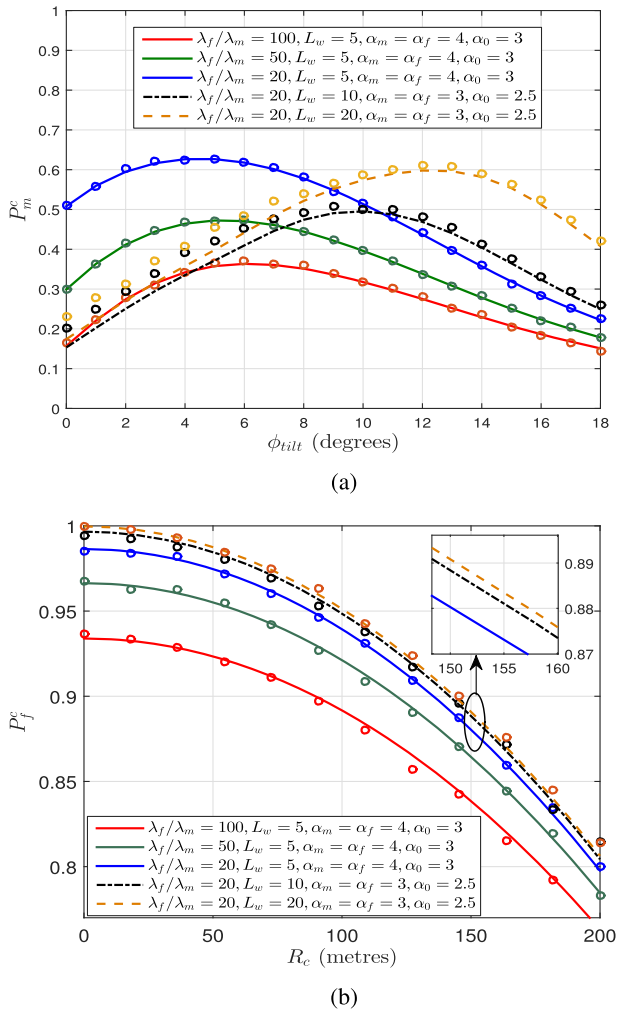

Fig. 4. Coverage probability of a heterogeneous network, with $\beta_m = \beta_f = 3$, $L_w = 5$ dB, $\alpha_m = \alpha_f = 4, \alpha_0 = 3, \lambda_m = 1.54 \text{ x } 10^{-6}$ (typicall hexagonal cell radius of 500 m.), and $\lambda_f/\lambda_m = 20$, 50 and 100 for (a) macrocell as a function of ϕ_{tilt} (with fixed $R_c = 200$ m), and (b) femtocell tier as a function of R_c.

interference from the femtocell tier has the effect of decreasing the value of the optimum tilt angle in comparison with a traditional network. We observe that the tilt angle that maximizes the coverage probability is highly dependent on both, the path loss exponent and the wall partition loss. In general, a higher value of L_w results in a higher value of the optimum tilt angle. This is due to the fact that a higher wall partition loss prevents interference from the femtocell to seriously affect the macrocell user performance, and so, the results resembles one of a macrocell-only network. Additionally, in general the smaller the path loss exponent, the highest the value of the antenna tilt angle. This also agrees with the behaviour previously described, in the sense that a smaller value of the path loss exponent results in an increase in the interference received from the femtocell tier. On the other hand, Fig. 4(b) shows the coverage probability for the femtocell tier as a function of the macrocell's guard zone R_c. As an increase in the size of R_c would prevent a larger number of femtocells from transmitting in the proximity of a macrocell user, the overall coverage in the femto tier is reduced. In this case, a smaller value of the path loss exponent results in an increase in the femtocell user performance. This is due

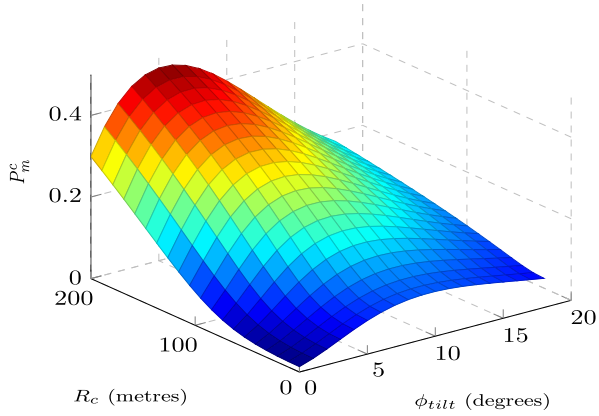

Fig. 5. Macrocell coverage probability as a function of ϕ_{tilt} and R_c with $\beta_m = \beta_f = 3$, $L_w = 5$ dB, $\alpha_m = \alpha_f = 4$, $\lambda_m = 1.54 \text{ x } 10^{-6}$ (typical hexagonal cell radius of 500 m), and $\frac{\lambda_f}{\lambda_m} = 50$.

to the small distances between a femtocell user and its serving FAP, for which a smaller path loss exponent results in a stronger signal received at the desired link, effectively increasing the performance. We also observe that the wall partition loss does not have such a strong effect on the femtocell tier as opposed to the case of the macrocell tier. This is due to the fact that the signal from an indoor FAP to another has to transverse through 2 walls. Moreover, the scenarios with wall partition loss of 10 dB and 20 dB present almost identical performances.

Fig. 5 shows two views of the coverage probability of the macrocell tier as a function of both, ϕ_{tilt} and R_c. It is evident that a bigger guard zone is desirable in this tier, as it would protect the macrocell users from a higher number of interferers. Also from Fig. 5, it can be seen that the tilt angle ϕ_{tilt} that maximizes the coverage probability varies with the size of R_c. In general, the values of ϕ_{tilt} in this scenario are smaller than the ones found for the traditional network, when the number of femtocells deployed is relatively small. On the other hand, increasing λ_f results in an increase on the tilt angle that maximizes the coverage in this tier.

Fig. 6 shows the EE for a two tier network as a function of R_c and ϕ_{tilt}. It can be seen that there is an antenna tilt angle that maximizes the EE for each value of R_c. Also, the smaller the value of R_c, the higher is the EE of the network. This is entirely related to the femtocell tier, given the fact that the femtocells provide high gains in the total throughput of the network, and so, with a higher number of active femtocells (smaller value of R_c), there are more gains in the EE of the system. However, as can be seen from 5, the coverage in the macrocell tier is highly sensitive to the interference created by the femtocells. Therefore, optimizing only with respect to the EE of the network would result in an unfair treatment of the macrocell tier. Therein lies the importance of the constraints in (35) to guarantee a minimum QoS in this tier.

The results from the optimization problem are presented in figures 7 to 9. Fig. 7 shows $\phi_{tilt}^{\star}$ as a function of the density of femtocells deployed per macrocell. It can be seen that for a small number of femtocells, the optimum tilt angle is also small. However, as the interference from the femtocell tier increases, the tilt angle that maximizes the EE (and satisfies

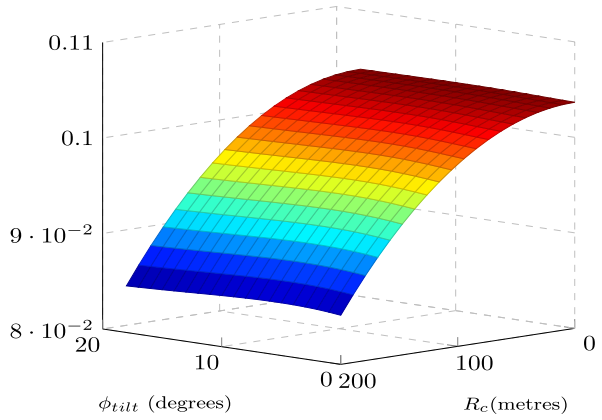

Fig. 6. Energy efficiency of a two tier network as a function of R_c and ϕ_{tilt} for a two tier network with $\beta_m = \beta_f = 3$, $L_w = 5$ dB, $\alpha_m = \alpha_f = 4$, $\alpha_0 = 3$, $\lambda_m = 1.54$ x 10^{-6} (typicall cell radius of 500 m), and $\frac{\lambda_f}{\lambda_m} = 50$.

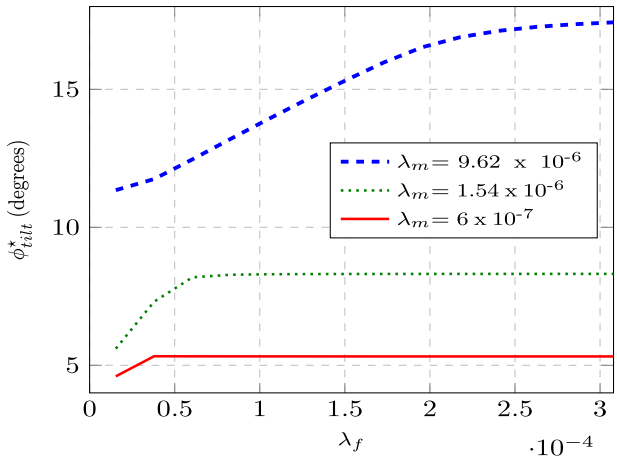

Fig. 7. Optimum tilt of a two tier network as a function of the density of femtocells for a two tier network with $L_w = 5$, $\beta_m = \beta_f = 3$, $\lambda_m = 9.6$ x 10^{-6}, 1.54 x 10^{-6} and 6 x 10^{-7}, $\epsilon_m = 0.3$ and $\epsilon_f = 0.8$.

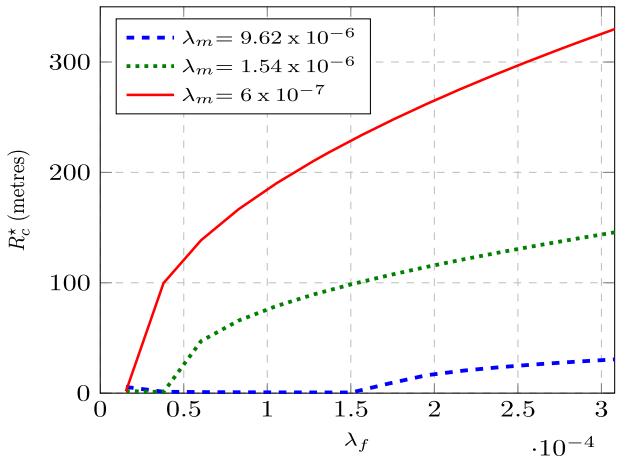

Fig. 8. Optimum R_c (i.e., R^*_c) of a two tier network as a function of the density of femtocells for a two tier network with $L_w = 5$, $\beta_m = \beta_f = 3$, $\lambda_m = 9.6$ x 10^{-6}, 1.54 x 10^{-6} and 6 x 10^{-7} m.), $\epsilon_m = 0.3$ and $\epsilon_f = 0.8$.

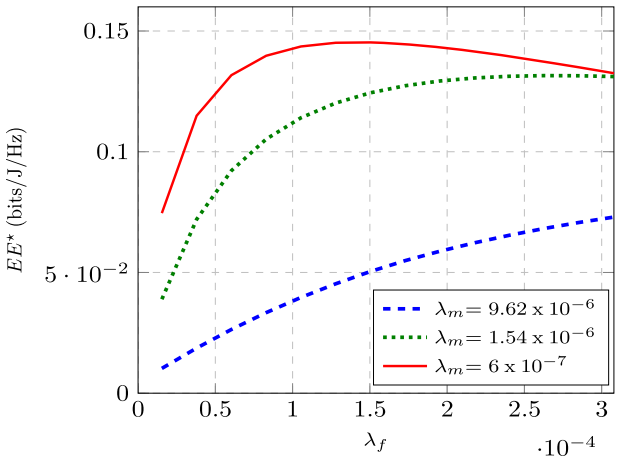

Fig. 9. Optimum energy efficiency of a two tier network as a function of the density of femtocells for a two tier network with $L_w = 5$, $\beta_m = \beta_f = 3$, $\lambda_m = 9.6$ x 10^{-6}, 1.54 x 10^{-6} and 6 x 10^{-7}, $\epsilon_m = 0.3$ and $\epsilon_f = 0.8$.

the constrains) increases until it settles at a fixed value when the number of femtocells deployed is high enough. Intuitively, as the number of femtocell increases, the edge users suffer the most damage to their received signal strength, and so a higher value for the tilt angle would steer the main lobe to an area closer to the edge of the cell to compensate for the interference from the femto tier.

Fig. 8 shows $R^{\star}_c$ as a function of the density of femtocells deployed per macrocell. As expected, as the number of femtocells increases, a bigger guard zone is required in order to protect the macrocell users from the femtocell tier interference.

Fig. 9 shows the optimum EE that complies with the constraints of the optimization problem when the density of femtocells per macrocell varies. It can be seen that when the number of femtocells increases from a small value, the EE of the network is significantly increased. This is in accordance with the overall expected gains in throughput in the network that come from having more femtocells deployed. However, if the number of femtocells deployed is too high, the maximum achievable EE_{max} first reaches a limit and then it starts to decay. This occurs when the interference starts to have a major effect and the gains in throughput are not as high as compared with the total power consumed in the network. In other words, the power consumed starts to outweigh the gains in throughput obtained by deploying a higher number of femtocells in the network. It is worthwhile to notice that even in the highest number of femtocells analysed in this work (200), the overall EE of the network is still superior to the case of the traditional network when the same value of λ_m is used. However, the performance in the macrocell tier in terms of the coverage is significantly reduced. This motivates the selection of the optimization parameters by the network designer in order to cope with the trade-off between the EE of the network and the coverage in the macrocell tier.

VI. Conclusion

In this work we provided a stochastic geometry framework to analize the performance of the network in terms of EE when the antenna tilt angle of macrocells is considered as an optimization parameter. In the case of a traditional network, we observe that our results can be easily scaled with regards to the density of

macrocells deployed in the network. As expected, the higher the density of macrocells, the bigger is the antenna tilt angle that optimizes the overall coverage and EE. In the case of a heterogeneous network consisting of macro- and femtocells we observe that even for a small number of femtocells deployed in the network, the performance of the macrocell user significantly decreases. Therefore, the use of a guard zone along with the tilt angle was proposed. From the results, it was verified that the EE of the network can be greatly increased by the inclusion of femtocells in comparison with a traditional network. However, the inclusion of femtocells using the same channel as a macrocell significantly deteriorates the performance of macrocell users. Therefore there must be a trade-off considering minimum QoS requirementes for the macrocell tier. In general, the optimum tilt angle that maximizes the EE of the network is smaller for a heterogeneous network compared with that obtained in a traditional network with the same macro base station density. Additionally, as the number of femtocells in the network increases, the optimum tilt angle decreases to compensate for the performance loss in the edge users. The presented model can be used as a starting point in the context of a Self Organising Network, where the number of femtocells can be greatly increased and with this information, the system can effectively adapt the tilt angle to obtain the best average performance in terms of the EE.

Appendix A
Derivation of P_m^c in (15)

First, we derive two important expressions that will help to express the final value of P_m^c. We take the general expression

$$\int_a^b \frac{y\,dy}{1+\frac{1}{B}\left(\frac{y}{r}\right)^{\alpha_m}} \tag{36}$$

where B can be any function not dependant on y. We proceed to find an alternative expression for (36). Similar to the analysis in [10], we make use of the substitution $u = (\frac{r_j}{rB^{\frac{1}{\alpha_m}}})^2$, and so

$$\int_a^b \frac{y\,dy}{1+\frac{1}{B}\left(\frac{y}{r}\right)^{\alpha_m}} = \int_{\left(\frac{a}{rB^{1/\alpha_m}}\right)^2}^{\left(\frac{b}{rB^{1/\alpha_m}}\right)^2} \frac{\left(rB^{\frac{1}{\alpha_m}}\right)^2 du}{1+u^{\frac{\alpha_m}{2}}}. \tag{37}$$

Now, the binomial negative series expansion is defined as

$$\begin{aligned}(c+x)^{-n} &= \sum_{k=0}^{\infty}\binom{-n}{k}x^k c^{-n-k}\\ &= \sum_{k=0}^{\infty}(-1)^k\binom{n+k-1}{k}x^k c^{-n-k}.\end{aligned} \tag{38}$$

Applying the definition in (38) to (37), with $c = u^{\frac{\alpha_m}{2}}$, $x = 1$ and $n = 1$, we obtain

$$\begin{aligned}&\int_a^b \frac{y\,dy}{1+\frac{1}{B}\left(\frac{y}{r}\right)^{\alpha_m}} \qquad (39)\\ &= \frac{\left(rB^{\frac{1}{\alpha_m}}\right)^2}{2}\sum_{k=0}^{\infty}\int_{\left(\frac{a}{rB^{1/\alpha_m}}\right)^2}^{\left(\frac{b}{rB^{1/\alpha_m}}\right)^2}(-1)^k\frac{(1)_k}{k!}\,u^{-\frac{\alpha_m(k+1)}{2}}du \qquad (40)\end{aligned}$$

where $(x)_k = \frac{\Gamma(x+k)}{\Gamma(x)} = x(x+1)...(x+k-1)$, is the Pochhammer symbol [39], and we used the property $(1)_k = k!$. Evaluating the integral on the R.H.S. of (40) we obtain

$$\begin{aligned}&\int_a^b \frac{y\,dy}{1+\frac{1}{B}\left(\frac{y}{r}\right)^{\alpha_m}}\\ &= \frac{\left(rB^{\frac{1}{\alpha_m}}\right)^2}{2}\left(\sum_{k=0}^{\infty}(-1)^k\frac{(1)_k}{k!}\,\frac{\left(\frac{a}{rB^{1/\alpha_m}}\right)^{-(1+k)\alpha_m+2}}{\frac{\alpha_m(k+1)}{2}-1}\right.\\ &\quad\left.-\sum_{k=0}^{\infty}(-1)^k\frac{(1)_k}{k!}\,-\frac{\left(\frac{b}{rB^{1/\alpha_m}}\right)^{-(1+k)\alpha_m+2}}{\frac{\alpha_m(k+1)}{2}-1}\right)\\ &= r^{\alpha_m}B\left(a^{2-\alpha_m}\sum_{k=0}^{\infty}(-1)^k\frac{(1)_k}{k!}\,\frac{\left(\left(\frac{a}{rB^{1/\alpha_m}}\right)^{-\alpha_m}\right)^k}{\alpha_m-2+k}\right.\\ &\quad\left.-b^{2-\alpha_m}\sum_{k=0}^{\infty}(-1)^k\frac{(1)_k}{k!}\,\frac{\left(\left(\frac{a}{rB^{1/\alpha_m}}\right)^{-\alpha_m}\right)^k}{\alpha_m-2+k}\right).\end{aligned} \tag{41}$$

By noting that $\frac{(x)_k}{(x+1)_k} = \frac{x}{x+k}$, with $x = \alpha_m - 2$, then (41) can be expressed as

$$\begin{aligned}&\int_a^b \frac{y\,dy}{1+\frac{1}{B}\left(\frac{y}{r}\right)^{\alpha_m}}\\ &= \frac{r^{\alpha_m}B}{\alpha_m-2}\left(a^{2-\alpha_m}\sum_{k=0}^{\infty}\frac{(1)_k}{k!}\,\frac{(\alpha_m-2)\left(-\left(\frac{a}{rB^{1/\alpha_m}}\right)^{-\alpha_m}\right)^k}{\alpha_m-2+k}\right.\\ &\quad\left.-b^{2-\alpha_m}\sum_{k=0}^{\infty}\frac{(1)_k}{k!}\,\frac{(\alpha_m-2)\left(-\left(\frac{a}{rB^{1/\alpha_m}}\right)^{-\alpha_m}\right)^k}{\alpha_m-2+k}\right).\end{aligned} \tag{42}$$

The summations in (42) correspond to the general expression of the hypergeometric function given by ${}_2F_1(a,b;c;x) = \sum_{k=0}^{\infty}\frac{(a)_k(b)_k}{(c)_k}\,\frac{(x)^k}{k!}$, and so using this expression we obtain

$$\begin{aligned}&\int_a^b \frac{y\,dy}{1+\frac{1}{B}\left(\frac{y}{r}\right)^{\alpha_m}}\\ &= \frac{r^{\alpha_m}B}{\alpha_m-2}\left(a_2^{2-\alpha_m}F_1\left(1,1-\frac{2}{\alpha_m};2-\frac{2}{\alpha_m};-\left(\frac{a}{r}\right)^{-\alpha_m}B\right)\right.\\ &\quad\left.-b_2^{2-\alpha_m}F_1\left(1,1-\frac{2}{\alpha_m};2-\frac{2}{\alpha_m};-\left(\frac{b}{r}\right)^{-\alpha_m}B\right)\right).\end{aligned} \tag{43}$$

In the special case in which $b = \infty$, (43) reduces to

$$\int_a^\infty \frac{y\,dy}{1+\frac{1}{B}\left(\frac{y}{r}\right)^{\alpha_m}} = \frac{r^{\alpha_m} B\, a^{2-\alpha_m}}{\alpha_m - 2}\, {}_2F_1\left(1, 1-\frac{2}{\alpha_m}; 2-\frac{2}{\alpha_m}; -\left(\frac{a}{r}\right)^{-\alpha_m} B\right). \tag{44}$$

Note that the expressions in (43) and (44) only hold when B is not a function of y, in which case we cannot find a closed form expression for (36). Now, as was stated in Section II, depending upon ϕ_{tilt}, we have two cases of antenna pattern expressions. For $\phi_{tilt} < \sqrt{A_{dB}/12}\,\phi_{3dB}$ we have the sum of two integrals expressed as

$$\begin{aligned} P_m^c = &\int_0^{r_{th1}} 2\pi\lambda_m \exp\left(-\lambda_m\pi\left\{r^2 + \frac{2}{N_s}\left[\int_r^{r_{th1}} \frac{y\,dy}{1+\frac{1}{\beta}\left(\frac{y}{r}\right)^{\alpha}} + \int_{r_{th1}}^{\infty} \frac{y\,dy}{1+\frac{G^{-1}(y)}{100\,\beta}\left(\frac{y}{r}\right)^{\alpha}}\right]\right\}\right) dr \\ &+ \int_{r_{th1}}^{\infty} 2\pi\lambda_m \exp\left(-\lambda_m\pi\left\{r^2 + \frac{2}{N_s}\int_r^{r_{th1}} \frac{y\,dy}{1+\frac{F^{-1}(ri)}{F^{-1}(r)\,\beta}\left(\frac{y}{r}\right)^{\alpha}}\right\}\right) dr. \end{aligned} \tag{45}$$

And for the case of $\phi_{tilt} \geq \sqrt{A_{dB}/12}\,\phi_{3dB}$, we have 3 integrals expressed as

$$\begin{aligned} P_m^c = &\int_0^{r_{th1}} 2\pi\lambda_m r \exp\left(-\lambda_m\pi\left\{r^2 + \frac{2}{N_s}\left[\int_r^{r_{th1}} \frac{y\,dy}{1+\frac{1}{\beta}\left(\frac{y}{r}\right)^{\alpha}} + \int_{r_{th1}}^{r_{th2}} \frac{y\,dri}{1+\frac{F^{-1}(y)}{100\,\beta}\left(\frac{y}{r}\right)^{\alpha}} + \int_{r_{th2}}^{\infty} \frac{y\,dy}{1+\frac{1}{\beta}\left(\frac{y}{r}\right)^{\alpha}}\right]\right\}\right) dr \\ &+ \int_{r_{th1}}^{r_{th2}} 2\pi\lambda_m r \exp\left(-\lambda_m\pi\left\{r^2 + \frac{2}{N_s}\int_r^{r_{th2}} \frac{y\,dy}{1+\frac{F^{-1}(y)}{F^{-1}(r)\,\beta}\left(\frac{y}{r}\right)^{\alpha}} + \int_{r_{th2}}^{\infty} \frac{y\,dy}{1+\frac{1}{\beta}\left(\frac{y}{r}\right)^{\alpha}}\right\}\right) dr \\ &+ \int_{r_{th2}}^{\infty} 2\pi\lambda_m r \exp\left(-\lambda_m\pi\left\{r^2 + \frac{2}{N_s}\int_r^{\infty} \frac{y\,dy}{1+\frac{F^{-1}(y)}{F^{-1}(r)\,\beta}\left(\frac{y}{r}\right)^{\alpha}}\right\}\right) dr. \end{aligned} \tag{46}$$

Substituting the expressions (43) and (44) previously found into (45) and (46), we obtain the results in (15), which concludes the proof.

Appendix B
Proof of $\mathcal{L}_{I_{\Phi'_f}}(\eta s)$ in (23)

From (22), we have

$$\mathcal{L}_{I_{\Phi'_f}}(\eta s) = \exp\left(-\lambda_f\pi\left\{(\eta s)^{\delta_f}\underbrace{E_h\left[h^{\delta_f}\gamma\left(1-\delta_f, \eta s h R_c^{-\alpha_f}\right)\right]}_{\xi} - \frac{R_c^2\eta s}{\eta s + R_c^{\alpha_f}}\right\}\right). \tag{47}$$

By using the definition of the incomplete Gamma function in ξ, we have

$$\xi = \int_0^\infty h^{\delta_f} e^{-h} \int_0^{\eta s h R_c^{-\alpha_f}} e^{-t} t^{-\delta_f}\,dt\,dh. \tag{48}$$

By using the substitution $x = t^{-1}(\eta s h R_c^{-\alpha_f})$, we obtain

$$\begin{aligned} \xi &= \left(\eta s R_c^{-\alpha_f}\right)^{1-\delta_f} \int_1^\infty x^{\delta_f - 2} \int_0^\infty h\, e^{-h\left(1+\frac{\eta s R_c^{-\alpha_f}}{x}\right)} dh\,dx \\ &= \left(\eta s R_c^{-\alpha_f}\right)^{1-\delta_f} \int_1^\infty \frac{x^{\delta_f-2}}{\left(1+\frac{\eta s R_c^{-\alpha_f}}{x}\right)^2} dx \\ &= \left(\eta s R_c^{-\alpha_f}\right)^{1-\delta_f} \int_1^\infty \frac{x^{\delta_f}}{\left(x+\eta s R_c^{-\alpha_f}\right)^2} dx. \end{aligned} \tag{49}$$

With the help of Maple, the integral can be evaluated in terms of the hypergeometric function, and so

$$\xi = \left(\eta s R_c^{-\alpha_f}\right)^{-\delta_f}\left(-\frac{1}{\eta s R_c^{-\alpha_f}+1} + {}_2F_1\left(1, -\delta_f; 1-\delta_f; -\eta s R_c^{-\alpha_f}\right)\right). \tag{50}$$

Substituting the value of (50) into (47), and after some more algebra we obtain

$$\mathcal{L}_{I_{\Phi'_f}}(\eta s) = e^{-\lambda_f\pi R_c^2\left({}_2F_1\left(1,-\delta_f;1-\delta_f;-\eta s R_c^{-\alpha_f}\right)-1\right)} \tag{51}$$

which concludes the evaluation.

References

[1] A. Damnjanovi *et al.*, "A survey on 3GPP heterogeneous networks," *IEEE Wireless Commun.*, vol. 18, no. 3, pp. 10–21, Jun. 2011.

[2] O. G. Aliu, A. Imran, M. A. Imran, and B. Evans, "A survey of self organisation in future cellular networks," *IEEE Commun. Surv. Tuts.*, vol. 15, no. 1, pp. 336–361, Feb. 2013.

[3] O. Yilmaz, S. Hamalainen, and J. Hamalainen, "Comparison of remote electrical and mechanical antenna downtilt performance for 3GPP LTE," in *Proc. IEEE 70th Veh. Technol. Conf. Fall (VTC'09 Fall)*, 2009, pp. 1–5.

[4] JDSU. (2013, Mar.). *Optimizing Small Cells and the Heterogeneous Network (HetNet)* [Online]. Available: http://www.jdsu.com/ProductLiterature/smallcellhetnet_wp_nsd_tm_ae.pdf
[5] M. Haenggi, J. G. Andrews, F. Baccelli, O. Sousse, and M. Franceschetti, "Stochastic geometry and random graphs for the analysis and design of wireless networks," *IEEE J. Sel. Areas Commun.*, vol. 27, no. 7, pp. 1029–1046, Sep. 2009.
[6] H. S. Dhillon, R. Krishna, F. Baccelli, and J. G. Andrews, "Modeling and analysis of k-tier downlink heterogeneous cellular networks," *J. Sel. Areas Commun.*, vol. 30, no. 3, pp. 550–560, Apr. 2012.
[7] W. C. Cheung, T. Q. S. Quek, and M. Kountouris, "Throughput optimization, spectrum allocation, and access control in two-tier femtocell networks," *IEEE J. Sel. Areas Commun.*, vol. 30, no. 3, pp. 561–574, Apr. 2012.
[8] R. W. Heath, M. Kountouris, and T. Bai, "Modeling heterogeneous network interference using Poisson point processes," *IEEE Trans. Signal Process.*, vol. 61, no. 16, pp. 4114–4126, Aug. 2013.
[9] H. El Sawy, E. Hossain, and M. Haenggi, "Stochastic geometry for modeling, analysis, and design of multi-tier and cognitive cellular wireless networks: A survey," *IEEE Commun. Surv. Tuts.*, vol. 15, no. 3, pp. 996–1019, Jul. 2013.
[10] J. G. Andrews, F. Baccelli, and R. Krishna, "A tractable approach to coverage and rate in cellular networks," *IEEE Trans. Commun.*, vol. 59, no. 11, pp. 3122–3134, Nov. 2011.
[11] B. Blaszczyszyn, M. Karray, and H. Keeler, "Using Poisson processes to model lattice cellular networks," in *Proc. IEEE INFOCOM*, Apr. 2013, pp. 773–781.
[12] A. Guo and M. Haenggi, "Spatial stochastic models and metrics for the structure of base stations in cellular networks," *IEEE Trans. Wireless Commun.*, vol. 12, no. 11, pp. 5800–5812, Nov. 2013.
[13] A. Imran *et al.*, "Distributed spectral efficiency optimization at hotspots through self organisation of BS tilts," in *Proc. IEEE GLOBECOM Workshops (GC Workshops)*, 2011, pp. 570–574.
[14] A. Imran, M. A. Imran, A. Abu-Dayya, and R. Tafazolli, "Self organization of tilts in relay enhanced networks: A distributed solution," *IEEE Trans. Wireless Commun.*, vol. 13, no. 2, pp. 764–779, Feb. 2014.
[15] W. Guo, S. Wang, Y. Wu, J. Rigelsford, X. Chu, and T. O'Farrell, "Spectral-and energy-efficient antenna tilting in a HetNet using reinforcement learning," in *Proc. IEEE Wireless Commun. Netw. Conf. (WCNC)*, 2013, pp. 767–772.
[16] A. Imran, M. Bennis, and L. Giupponi, "Use of learning, game theory and optimization as biomimetic approaches for self-organization in macro-femtocell coexistence," in *Proc. Wireless Commun. Netw. Conf. Workshops (WCNCW)*, 2012, pp. 103–108.
[17] H. Wang and M. C. Reed, "Tractable model for heterogeneous cellular networks with directional antennas," in *Proc. Aust. Commun. Theory Workshop (AusCTW)*, 2012, pp. 61–65.
[18] J. Wildman, P. H. J. Nardelli, M. Latva-Aaho, and S. Weber, "On the joint impact of beamwidth and orientation error on throughput in wireless directional Poisson networks," *CoRR*, vol. abs/1312.6057, 2013 [Online]. Available: http://arxiv.org/abs/1312.6057
[19] T. Bai and R. Heath, "Coverage and rate analysis for millimeter wave cellular networks," *IEEE Trans. Wireless Commun.*, vol. 14, no. 2, pp. 1100–1114, Feb. 2015.
[20] M. Di Renzo, "Stochastic geometry modeling and analysis of multi-tier millimeter wave cellular networks," *IEEE Trans. Wireless Commun.*, vol. 14, no. 9, pp. 5038–5057, May 2015.
[21] W. Lu and M. Di Renzo, "Stochastic geometry modeling of cellular networks: Analysis, simulation and experimental validation," *arXiv preprint arXiv:1506.03857*, 2015.
[22] 3GPP, "Further advancements for E-UTRA physical layers aspects (release 9)," 3GPP, Sophia Antipolis, France, Tech. Rep. TR36.814 v9.0.0, Mar. 2010.
[23] T. M. Nguyen, Y. Jeong, T. Q. S. Quek, W. P. Tay, and H. Shin, "Interference alignment in a Poisson field of mimo femtocells," *IEEE Trans. Wireless Commun.*, vol. 12, no. 12, pp. 2633–2645, Jun. 2013.
[24] V. Chandrasekhar and J. G. Andrews, "Spectrum allocation in tiered networks," *IEEE Trans. Commun.*, vol. 57, no. 10, pp. 3059–3068, Oct. 2009.
[25] H.-S. Jo, P. Xia, and J. G. Andrews, "Downlink femtocell networks: Open or closed?," in *Proc. IEEE Int. Conf. Commun. (ICC)*, Jun. 2011, pp. 1–5.
[26] S. Chen, H. Jin, Y. Li, and M. Peng, "Performance analysis of two-tier femtocell networks in Nakagami-m fading channels," in *Proc. Int. Conf. Wireless Commun. Signal Process. (WCSP)*, 2013, pp. 1–5.
[27] 3GPP, "Evolved universal terrestrial radio access (E-UTRA); Further advancements for E-UTRA physical layer aspects," 3GPP, Sophia Antipolis, France, Tech. Rep. TR 36.814 v0.4.1.
[28] D. Stoyan, W. S. Kendall, and J. Mecke, *Stochastic Geometry and Its Applications*, 2nd ed. Hoboken, NJ, USA: Wiley, 1995.
[29] S.-M. Cheng, W. C. Ao, F.-M. Tseng, and K.-C. Chen, "Design and analysis of downlink spectrum sharing in two-tier cognitive femto networks," *IEEE Trans. Veh. Technol.*, vol. 61, no. 5, pp. 2194–2207, Jun. 2012.
[30] M. Haenggi and K. Ganti, *Interference in Large Wireless Networks*. Delft, The Netherlands: NOW, 2009.
[31] M. Haenggi, "Mean interference in hard-core wireless networks," *IEEE Commun. Lett.*, vol. 15, no. 8, pp. 792–794, Aug. 2011.
[32] A. J. Fehske, F. Richter, and G. P. Fettweiss, "Energy efficiency improvements through micro sites in cellular mobile radio networks," in *Proc. GLOBECOM Workshops*, Nov. 2009, pp. 1–5.
[33] H. Klessig, A. J. Fehske, and G. Fettweis, "Energy efficiency gains in interference-limited heterogeneous cellular mobile radio networks with random micro site deployment," in *Proc. IEEE Sarnoff Symp.*, May 2011, pp. 1–6.
[34] M. Deruyck, D. D. Vulder, W. Joseph, and L. Martens, "Modelling the power consumption in femtocell networks," in *Proc. WCNC Workshop Future Green Commun.*, Apr. 2012, pp. 30–35.
[35] Kathrein Inc (2015), "800 10290V01 antenna specifications," [Online]. Available: http://www.kathrein-scala.com/catalog/80010290V01.pdf
[36] Alliance corporation. (2015). *Andrew® Tri-Band Antenna TBXLHB-6565a-VTM Specifications*, Alliance Corporation [Online]. Available: http://latex-community.org/forum/viewtopic.php?f=48&t=4328
[37] 4G Americas. (2012, Oct.). *Mimo and Smart Antennas for Mobile Broadband Systems* [Online]. Available: http://www.4gamericas.org/files/2114/0759/4301/MIMO_and_Smart_Antennas_for_Mobile_Broadband_Systems_Oct_2012x.pdf
[38] CommScope Inc. (2015). *Andrew® Metrocell Antenna Specifications*, CommScope Inc. [Online]. Available: http://www.commscope.com/catalog/andrew/product_details.aspx?id=34914
[39] I. Gradshteyn and I. Ryzhik, *Table of Integrals, Series, and Products*, 7th ed. Amsterdam, The Netherlands: Elsevier, 2007.

Raul Hernandez-Aquino received the degree (cum laude) in electronic and communications engineering from the Universidad De Las Americas Puebla (UDLAP), Cholula, Mexico, in 2008, and the M.Sc. degree in electronics (major in telecommunications) from the Instituto Tecnologico y de Estudios Superiores de Monterrey (ITESM), Monterrey, Mexico, in 2012. Currently, he is pursuing the Ph.D. degree in telecommunications at the University of Leeds, Leeds, U.K. In 2008, he worked as a Research Engineer with the Instituto Nacional de Astrofisica, Optica y Electronica (INAOE), Puebla, Mexico and was an Attendant to the information and communication technology formation program, T-Systems Mexico, Puebla, Mexico where he received five certifications as Server Administrator (from Microsoft and Sun Microsystems). He worked as a System Administrator with T-Systems Mexico, from February to December 2009. He is the coauthor of the "Network Management and Traffic Engineering," a chapter of the book *Building Next-Generation Converged Networks: Theory and Practice* (Taylor & Francis, 2013). His research interests include broadly communication theory, heterogeneous networks, and signal processing for communications.

Syed Ali Raza Zaidi (S'09) received the B.Eng. degree in information and communication system engineering from the School of Electronics and Electrical Engineering, NUST, Islamabad, Pakistan, in 2008. Currently, he is pursuing the Ph.D. degree at the School of Electronics and Electrical Engineering, University of Leeds, Leeds, U.K. Currently, he is a Research Fellow on the U.S. Army Research Lab funded project with the University of Leeds. From September 2007 to August 2008, he served as a Research Assistant with Wireless Sensor Network Lab on a collaborative research project between NUST and Ajou University, South Korea. He was a Visiting Research Scientist at Qatar Innovations and Mobility Centre from October to December 2013. His research interests include design and analysis of the large scale ad-hoc wireless networks employing tools from stochastic geometry and random graph theory. He has served as an Invited Reviewer for the IEEE Flagship journals and conferences. He is also U.K. Liasion for the European Association for Signal Processing (EURASIP). He has served on the program committees and as a Chair in

various IEEE Flagship Conferences. He is the Technical Program Chair for the EAI STEMCOM 2016 and Workshop Chair for the IEEE CAMAD 2015 special session on Performance Analysis and Modelling of Large-Scale 5G Networks, IEEE WCMC 2015 workshop on Recent Advances at Physical Layer for 5G Wireless Networks, and the IEEE VTC workshop on Emerging Device Centric Communication. He has also served as a Track Chair for Theory and Modeling Track at the IEEE/ICST CROWNCOM 2015. He is also a Lead Guest Editor for the IET Signal Processing SI on Recent Advances in Signal Processing for 5G Wireless Networks and Associate Editor for the IEEE COMMUNICATION LETTERS. He was the recipient of the NUSTs most prestigious Rectors Gold Medal for his final year project and was also the recipient of the Overseas Research Student Scholarship along with Tetley Lupton and Excellence Scholarships, in 2008, to pursue his Ph.D. degree. He was also was the recipient of the COST IC0902, DAAD, and Royal Academy of Engineering Grants to promote his research.

Des McLernon (M'94) received the B.Sc. degree in electronic and electrical engineering and the M.Sc. degree in electronics from Queens University of Belfast, Northern Ireland, U.K., and the Ph.D. degree in signal processing from the Imperial College, University of London, London, U.K. He then worked on radar research and development with Ferranti Ltd., Edinburgh, Scotland, and later joined the Imperial College, University of London. After first lecturing at South Bank University, London, U.K., he moved to the School of Electronic and Electrical Engineering, University of Leeds, Leeds, U.K., where he is a Reader in signal processing. He has authored over 280 journal and conference papers in the domain of signal processing for communications. His research interests include the domain of signal processing for communications.

Mounir Ghogho (SM'96) received the M.Sc. and Ph.D. degrees from the National Polytechnic Institute of Toulouse, Toulouse, France, in 1993 and 1997, respectively. He was an EPSRC Research Fellow with the University of Strathclyde, Glasgow, Scotland, from September 1997 to November 2001. Since December 2001, he has been a Faculty Member with the School of Electronic and Electrical Engineering, University of Leeds, Leeds, U.K. where he currently holds a Chair in signal processing and communications. Since 2010, he has also been a Research Director with the International University of Rabat, Technopolis, Morocco. He has authored over 250 journal and conferences papers. His research interests include signal processing and communication networks. Currently, he is an Associate Editor of the *IEEE Signal Processing Magazine*. From 2005 to 2008, he served as an Associate Editor of the IEEE TRANSACTIONS ON SIGNAL PROCESSING; from 2001 to 2004, the IEEE SIGNAL PROCESSING LETTERS, and *Digital Signal Processing* (Elsevier), from 2011 to 2012. Currently, he is a Member of the IEEE Signal Processing Society SAM Technical Committee. He served as a Member of the IEEE Signal Processing Society SPCOM Technical Committee from 2005 to 2010 and a Member of IEEE Signal Processing Society SPTM Technical Committee from 2006 to 2011. He was the General Chair of the 11th IEEE workshop on Signal Processing for Advanced Wireless Communications (SPAWC2010), General Chair of the 21st edition of the European Signal Processing Conference (EUSIPCO 2013), the Technical Co-Chair of the MIMO symposium of IWCMC 2007 and IWCMC 2008. He held the Invited Scientist/Professor positions with many institutions including the U.S. Army Research Lab, USA; Tlcom Paris-Tech, France; National Institute of Informatics, Japan; the University Carlos Third of Madrid, Spain; ENSICA, France; Technical University of Darmstadt, Germany; the University of Minnesota, USA; Beijing University of Posts and Telecommunication, China; and the University Mohamed V, Morocco. He is the EURASIP Liaison in Morocco. He was the recipient of the U.K. Royal Academy of Engineering Research Fellowship in September 2000 and was also the recipient of the 2013 IBM Faculty Award.

Ali Imran (M'xx) is an Assistant Professor in telecommunications with the University of Oklahoma, Norman, OK, USA. Currently, he is leading a multinational $1.045 million research project on Self Organizing Cellular Networks, QSON (www.qson.org). He has authored over 50 peer-reviewed articles and has presented number of tutorials at international forums such as IEEE ICC, IEEE WCNC, European Wireless, and CrownCom on these topics. His research interests include self-organizing networks, radio resource management, and big data analytics. He is an Associate Fellow of Higher Education Academy (AFHEA), U.K. and Member of Advisory Board to Special Technical Community on Big Data with the IEEE Computer Society.